Available online at www.sciencedirect.com
ScienceDirect
Continental Shelf Research 28 (2008) 112–136
CONTINENTAL SHELF RESEARCH
www.elsevier.com/locate/csr

A three-dimensional biophysical model of *Karenia brevis* dynamics on the west Florida shelf: A look at physical transport and potential zooplankton grazing controls

Scott P. Milroy[a,*], Dwight A. Dieterle[a], Ruoying He[b], Gary J. Kirkpatrick[c], Kristen M. Lester[d], Karen A. Steidinger[e], Gabriel A. Vargo[a], John J. Walsh[a], Robert H. Weisberg[a]

[a]*College of Marine Science, University of South Florida, 140 Seventh Avenue S, St. Petersburg, FL 33701, USA*
[b]*Woods Hole Oceanographic Institution, Mail Stop 10, Woods Hole, MA 02543, USA*
[c]*Mote Marine Laboratory, 1600 Ken Thompson Parkway, Sarasota, FL 34236, USA*
[d]*Lyme Academy, 84 Lyme Street, Old Lyme, CT 06371, USA*
[e]*Fish and Wildlife Research Institute, Florida Fish and Wildlife Conservation Commission, 100 Eighth Avenue SE, St. Petersburg, FL 33701, USA*

Received 26 May 2004; received in revised form 10 January 2007; accepted 10 April 2007
Available online 22 July 2007

Abstract

The development of accurate predictive models of toxic dinoflagellate blooms is of great ecological importance, particularly in regions that are most susceptible to their detrimental effects. This is especially true along the west Florida shelf (WFS) and coast, where episodic bloom events of the toxic dinoflagellate *Karenia brevis* often wreak havoc on the valuable commercial fisheries and tourism industries of west Florida. In an effort to explain the dynamics at work within the maintenance and termination phases of a red tide, a simple three-dimensional coupled biophysical model was used in the analysis of the October 1999 red tide offshore Sarasota, Florida. Results of the numerical experiments indicate that: (1) measured and modeled flowfields were capable of transporting the observed offshore inoculum of *K. brevis* to within 16 km of the coastal boundary; (2) background concentrations (1000 cells L^{-1}) of *K. brevis* could grow to a red tide of over 2×10^6 cells L^{-1} in little more than a month, assuming an estuarine initiation site with negligible offshore advection, no grazing losses, negligible competition from other phytoplankton groups, and no nutrient limitation; (3) maximal grazing pressure could not prevent the initiation of a red tide or cause its termination, assuming no other losses to algal biomass and a zooplankton community ingestion rate similar to that of *Acartia tonsa*; and (4) the light-cued ascent behavior of *K. brevis* served as an aggregational mechanism, concentrating *K. brevis* at the 55 μE m^{-2} s^{-1} isolume when mean concentrations of *K. brevis* exceeded 100,000 cells L^{-1}. Further improvements in model fidelity will be accomplished by the future inclusion of phytoplankton competitors, disparate nutrient availability and limitation schemes, a more realistic rendering of the spectral light field and the attendant effects of photo-inhibition and compensation, and a mixed community of vertically-migrating proto- and metazoan grazers. These model refinements are currently under development and shall be used to aid progress toward an operational model of red tide forecasting along the WFS.

Keywords: Mathematical models; Red tides; Algal blooms; Phytoplankton; *Karenia brevis*

*Corresponding author. Tel.: +1 727 553 1112; fax: +1 727 553 1189.
E-mail address: smilroy@seas.marine.usf.edu (S.P. Milroy).

0278-4343/$ - see front matter © 2007 Elsevier Ltd. All rights reserved.
doi:10.1016/j.csr.2007.04.013

1. Introduction

The development of accurate predictive models of toxic dinoflagellate blooms is of great ecological and financial importance, particularly in regions that are most susceptible to their detrimental effects. This is especially true along the west Florida shelf (WFS) and coast, where episodic bloom events of the unarmored dinoflagellate *Karenia brevis* (= *Gymnodinium breve*, *Ptychodiscus brevis*) can cause mass mortalities of over 100 species of marine life (Steidinger and Ingle, 1972; Steidinger, 1983; Sakamoto et al., 1987), the results of which often wreak havoc on the valuable commercial fisheries and tourism industries of west Florida. The red tide organism *K. brevis* has been linked to these mortalities either directly due to the production and release of a variety of neurotoxins (Shimizu et al., 1995) or indirectly due to the depletion of dissolved oxygen during respiration (Simon and Dauer, 1972). The bioaccumulation of sub-lethal brevitoxins in fish and mollusk tissues has led to significant dolphin and seabird mortalities (Steidinger and Haddad, 1981) and has even been linked to neurotoxic shellfish poisoning (NSP) in humans (Shimizu et al., 1986). Brevitoxins released from lysed cells may also become airborne, and in the presence of breaking waves and/or onshore winds, may cause severe respiratory irritation to humans along the coast (Pierce et al., 1990). Thus, when considering the multitude of ecological, commercial, and public health hazards associated with these blooms, a reliable model of *K. brevis* population dynamics could be used to forecast the severity, location, and subsequent transport of red tides in an effort to mitigate ecological and financial losses incurred therefrom.

Until recently, the causative elements that underlie the initiation and dispersal of red tides had remained enigmatic. While several paradigms have been developed in past decades, they have all sought to reduce the complexities of toxic dinoflagellate ecology to a simple index of one or very few requisite environmental predictors. To date, red tides have been linked to the anthropogenic eutrophication of coastal waters (Satsmadjis and Friligos, 1983; Cannon, 1990; Pagou and Ignatiades, 1990), increased estuarine efflux (Chew, 1956), warm temperatures (Chew, 1956; Fraga et al., 1990; Pagou and Ignatiades, 1990), salinities of 21–37 psu (Rounsefell and Dragovich, 1966; Wilson, 1967), periods of decreased vertical mixing (Margalef et al., 1979; Cannon, 1990; Wyatt, 1990), and proximity to density fronts (Margalef et al., 1979; Taft and Martin, 1986; Fraga et al., 1990; Franks, 1992).

However, several investigations of *K. brevis* bloom dynamics in the eastern Gulf of Mexico and on the WFS have indicated that *K. brevis* is not normally a coastally occurring species. Rather, it is indigenous to oligotrophic shelf waters (Steidinger and Haddad, 1981; Tester and Steidinger, 1997), where blooms are instead thought to originate 18–74 km offshore (Steidinger, 1973; Steidinger, 1975; Steidinger and Haddad, 1981) since the nutrient-replete conditions in nearshore waters will instead favor blooms of diatoms and other phytoplankton competitors (Walsh et al., 2003).

While previous one-dimensional (Penta, 2000) and three-dimensional (Walsh et al., 2001, 2002, 2003) models have offered a great deal of insight into *K. brevis* dynamics on the WFS, it is difficult to embark upon exhaustive ecological simulations without a robust data set to initialize and validate such models. Fortunately, hydrographic data from several cruises on the WFS during August–November 1999 were available for the development of these models, including measures of:

(1) Biophysical and biooptical oceanographic parameters, such as temperature, salinity, density, light attenuation, and transmission (Ecology and Oceanography of Harmful Algal Bloom—ECOHAB, Mote, NEGOM, HRS, HyCODE);
(2) *In situ* nutrient concentrations, including ammonia, nitrate, nitrite, phosphate, silicate, and dissolved organic nitrogen–DON (ECOHAB, Mote, NEGOM);
(3) *In vivo* chlorophyll-*a* data (ECOHAB, Mote, NEGOM);
(4) Offshore and coastal *K. brevis* cell counts (ECOHAB, Mote, FMRI); and
(5) Zooplankton diversity, biomass, and abundance (HRS, ECOHAB).

Indeed, red tide dynamics on the WFS have been shown to be anything but simple, requiring a complex analysis of the biological, chemical, and physical contributions *in toto*. Walsh et al. (2006) have elucidated several complex requisites for the successful competition of *K. brevis*, whereby the initiation and persistence of red tides follow a strict chronology, requiring:

(1) A mid-shelf, phosphorus-rich nutrient supply (at low dissolved inorganic nitrogen (DIN)/dissolved inorganic phosporus (DIP) ratios)

(2) Aeolian delivery of iron-rich dust to alleviate diazotroph Fe-limitation
(3) Relaxation of N-limitation due to diazotroph release of DON
(4) Co-aggregation of sun-adapted diazotrophs and shade-adapted *K. brevis*
(5) Vertical migration of *K. brevis* into near-bottom Ekman layers
(6) Coastal upwelling of *K. brevis* into coastal, CDOM-rich surface waters
(7) Release of ichthyotoxic exudates from *K. brevis*, causing fish kills
(8) *In situ* growth of self-shaded *K. brevis*, fed by decaying diazotrophs/fish

While the biophysical model proposed by Walsh et al. (2006) has been used to explain the initiation of red tides from background concentrations on the WFS, the factors affecting bloom maintenance are less well known than those of onset.

1.1. Objectives

During the course of these Fall 1999 studies, a deep patch of *K. brevis* (33,000 cells L^{-1}) was sampled in the near-bottom waters at the 30-m isobath offshore Sarasota on 30 August 1999, just 37 days prior to a large bloom event (5.9×10^6 cells L^{-1}) observed at the coast during 04–08 October 1999 (Fig. 1). If the deep-water patch of *K. brevis* was indeed the inoculum for the coastal bloom event, it would have required the vertical migration of *K. brevis* into the near-bottom Ekman layers and subsequent advection into near-shore waters during a period of coastal upwelling. This paradigm would also require a light and nutrient climate favorable to the net growth of the *K. brevis* biomass on the inner shelf, particularly in light of potential losses due to zooplankton grazing.

To explore the events affecting the maintenance and inshore transport of a red tide initiated offshore, significant modifications to the Walsh et al. (2002) model were made in an effort to simulate the October 1999 red tide offshore Sarasota, Florida while addressing the following key questions:

(1) Are the measured and modeled flow fields of a magnitude and direction such that the small red tide observed 46 km offshore could be advected onshore in keeping with observed events?
(2) Is *in situ* growth of *K. brevis* sufficient to reach the observed bloom proportions without having to invoke aggregational paradigms?
(3) To what extent was zooplankton grazing a significant contributor to the mitigation and/or termination of the red tide?

2. Methods

2.1. Initialization and validation of the biophysical model

Cross-shelf sections were taken to the 1000 m isobath within the eastern Gulf of Mexico throughout the summer/fall of 1999 as a part of the concurrent NOAA/EPA ECOHAB, Mote Marine Laboratory (Mote), USF Ocean Circulation Group (OCG), and Florida Marine Research Institute (FMRI) research initiatives (Fig. 2). All hydrographic datNO_3^-a were determined from CTD casts at discrete stations, except for surface *K. brevis* cell counts at select coastal stations (FMRI) and satellite-relayed telemetry from moored ADCP arrays (OCG). Inorganic nutrients (SiO_4, , NH_4^+, PO_4^{3-}) were determined at micromolar levels using standard methods (Atlas et al., 1971; Gordon et al., 1994). Extracted chlorophyll stocks were measured with both the Holm–Hansen/Welschmeyer fluorometric protocols (Heil et al., 2002) and HPLC assays (Wright et al., 1991), which yielded similar estimates of the chlorophyll-*a* concentrations. Ultimately, these data were used to establish the initial and boundary conditions for the variety of state variables computed within the biophysical model.

2.2. Physical forcing

The physical circulation model used to resolve time-dependent flows on the WFS is a modification of the original Blumberg and Mellor (1987) Princeton Ocean Model (POM), and has been used extensively to model WFS circulation (Li and Weisberg, 1999a, b; He and Weisberg, 2002, 2003). The WFS-POM (see Table 1 for a list of the physical model parameters) consists of a domain which extends from the Florida Keys to the Mississippi River delta (Fig. 3), partitioned into an orthogonal curvilinear grid with a horizontal resolution varying between ~2 km near the coast and ~6 km near the open boundary (He and Weisberg, 2003). A topography-following sigma coordinate system, where $\sigma = (z-\eta)\ (H+\eta)^{-1}$, is employed in the vertical dimension with 21 layers distributed non-uniformly to better resolve the near-surface and near-bottom boundary layers (He and Weisberg,

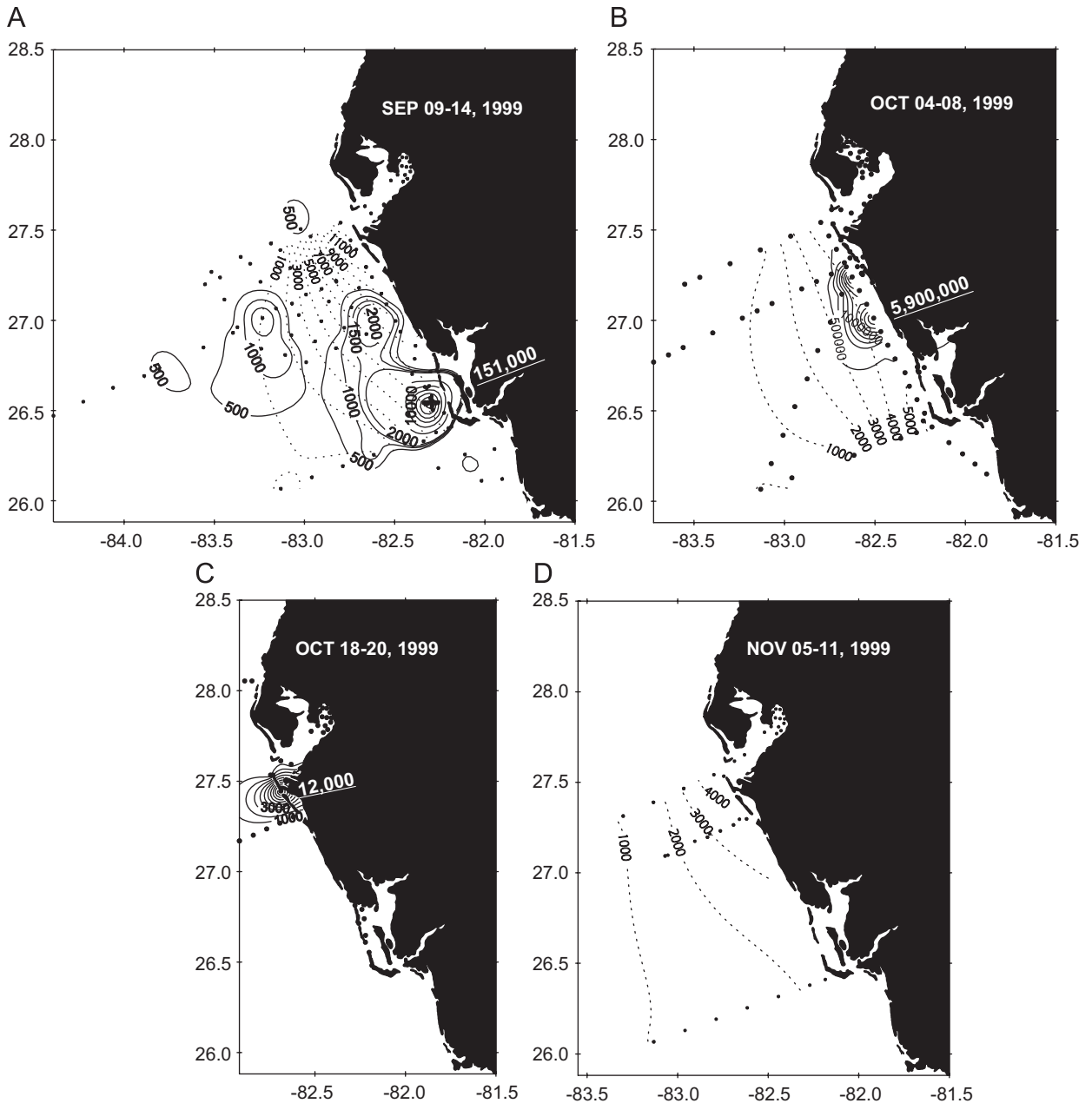

Fig. 1. Stocks of *K. brevis* and zooplankton observed during ECOHAB, Mote, and FMRI red tide sampling for (A) September 09–14; (B) October 04–08; (C) October 18–20; and (D) November 05–11, 1999. Solid lines indicate *K. brevis* surface concentrations (cells L^{-1}). Broken lines indicate the depth-averaged abundance of adult zooplankton (individuals m^{-3}).

2002, 2003). The equations governing general shelf circulation and surface elevation are:

$$\frac{\partial(DU)}{\partial x}+\frac{\partial(DV)}{\partial y}+\frac{\partial \omega}{\partial \sigma}+\frac{\partial \eta}{\partial t}=0, \tag{1}$$

$$\frac{\partial(UD)}{\partial t}+\frac{\partial(UUD)}{\partial x}+\frac{\partial(UVD)}{\partial y}+\frac{\partial(U\omega)}{\partial \sigma}-fVD + gD\frac{\partial \eta}{\partial x}=\frac{\partial}{\partial \sigma}\left(\frac{K_M}{D}\frac{\partial V}{\partial \sigma}\right)+F_x, \tag{2}$$

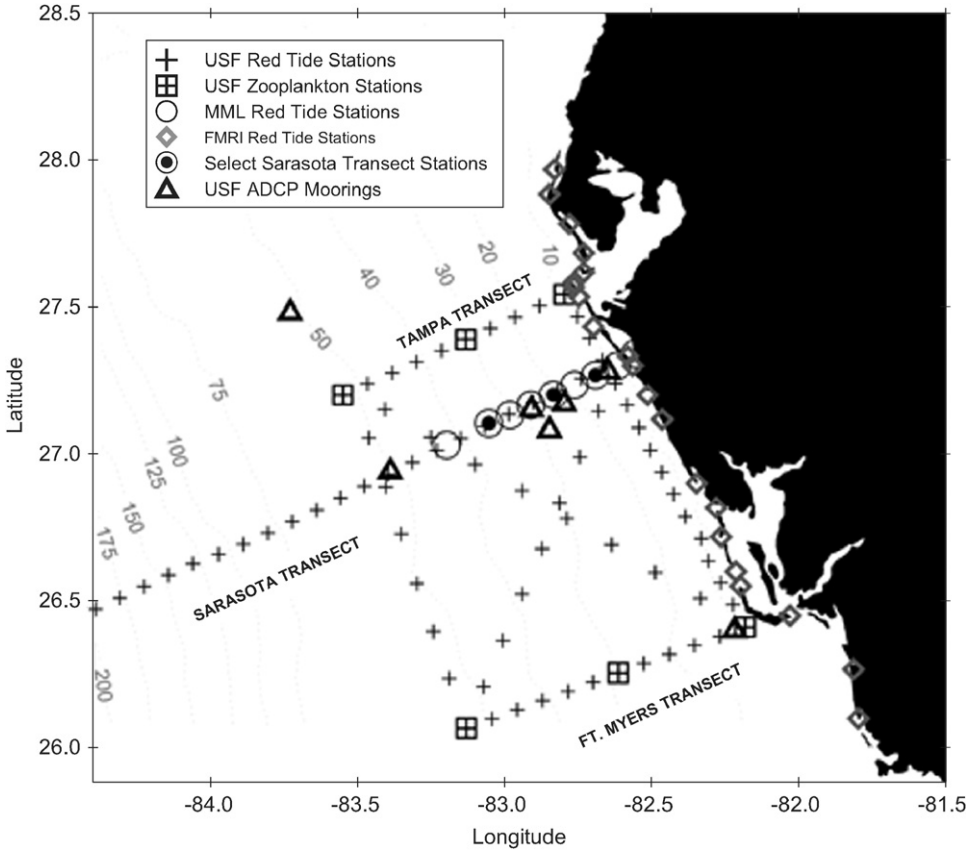

Fig. 2. Geographic location of the ECOHAB, Mote, and FMRI red tide transects and individual stations along the west Florida shelf (WFS), including ADCP moorings. Broken lines indicate WFS bathymetry (meters).

$$\frac{\partial(VD)}{\partial t}+\frac{\partial(UVD)}{\partial x}+\frac{\partial(VVD)}{\partial y}+\frac{\partial(V\omega)}{\partial \sigma}+fUD + gD\frac{\partial \eta}{\partial y}=\frac{\partial}{\partial \sigma}\left(\frac{K_M}{D}\frac{\partial V}{\partial \sigma}\right)+F_y, \tag{3}$$

where the horizontal friction terms are defined as

$$F_x=\frac{\partial}{\partial x}(D\tau_{xx})+\frac{\partial}{\partial y}(D\tau_{yx}), \tag{4}$$

$$F_y=\frac{\partial}{\partial x}(D\tau_{xy})+\frac{\partial}{\partial y}(D\tau_{yy}), \tag{5}$$

such that

$$\tau_{xx}=2A_M\frac{\partial U}{\partial x}, \tag{6}$$

$$\tau_{xy}=\tau_{yx}=A_M\left(\frac{\partial U}{\partial y}+\frac{\partial V}{\partial x}\right), \tag{7}$$

$$\tau_{yy}=2A_M\frac{\partial V}{\partial y}. \tag{8}$$

The model is forced by wind, air pressure, and net surface heat flux fields from the National Center for Environment Prediction (NCEP) plus freshwater mass fluxes from the Mississippi, Mobile, Apalachicola, Suwannee, Hillsborough, Peace, and Shark rivers (He and Weisberg, 2003). Tidal forcing is excluded since previous (Li and Weisberg, 1999a, b; He and Weisberg, 2002) modeling investigations have shown that the related tidal mixing is weak in comparison with other sources for mixing.

The model uses an Arakawa C grid conserving both linear and quadratic quantities such as mass and energy (Yang and Weisberg, 1999). A mode-splitting technique was employed to solve the two-dimensional external mode equations in short (12 s) time steps, while the three-dimensional internal mode equations were solved in longer (360 s) time steps (Yang and Weisberg, 1999; Walsh et al., 2002), both of which fall within the Courant–Friedrichs–Levy (CFL) stability constraints (Roach, 1976). Horizontal diffusivities are parameterized according

Table 1
Physical and biological variables in the coupled biophysical model of *K. brevis* on the west Florida shelf

σ	Sigma coordinate
x, y	Cartesian horizontal coordinates
z	Cartesian vertical coordinate
η	Free sea surface height relative to mean sea level
H	Water depth relative to mean sea level
U	Horizontal velocity component in the east/west direction
V	Horizontal velocity component in the north/south direction
D	Instantaneous water depth
ω	Vertical velocity component normal to the sigma surface
t	Time
f	Coriolis (varies from 5.77×10^{-5} to $7.48\times10^{-5}\,s^{-1}$)
g	Acceleration due to gravity ($9.8\,m\,s^{-2}$)
K_H	Vertical kinematic viscosity
F_x, F_y	Horizontal friction components
τ_x, τ_y	Horizontal wind stress components
A_M	Horizontal viscosity
ρ_0	Density of seawater
C_z	Vertical shear constant
k	von Karman constant (0.4)
σ_{kb-1}	Sigma layer next to the seafloor
z_0	Roughness parameter
$Tr[B]$	Physical advective and diffusive transport of state variable "B"
P	Carbon-specific phytoplankton biomass
μ^*	Realized net growth rate
e	Excretion loss coefficient
g	Grazing loss coefficient
l	Lysis loss coefficient
w	Sinking velocity
K_z	Vertical eddy diffusivity
μ_L	Light-limited growth rate
$\mu_{(T)}$	Temperature-dependent maximal growth rate
μ_M	Maximum theoretical growth rate at 27 °C
T	Temperature
I_z	Irradiance at depth
I_{sat}	Saturation Irradiance
I_0	Irradiance at the water surface
k_z	Attenuation coefficient
${}^{B}a_w$	Coefficient of "blue-light" attenuation due to seawater ($0.04348\,m^{-1}$)
${}^{R}a_w$	Coefficient of "red-light" attenuation due to seawater ($0.04000\,m^{-1}$)
a_c	Coefficient of attenuation due to CDOM
a_{chl}	Attenuation coefficient due to *K. brevis* chlorophyll ($0.01400\,mg^{-1}\,chl\,m^2$)
chl	Chlorophyll concentration ($mg\,L^{-1}$)
a_z	Coefficient of attenuation at depth z
${}^{R}FRAC_{\mathrm{I}}$	Fraction of surface irradiance divided into the "red band" (0.5)
${}^{B}FRAC_{\mathrm{I}}$	Fraction of surface irradiance divided into the "blue band" (0.5)
${}^{R}\mathrm{I}_z$	"Red-light" Irradiance at depth z
${}^{B}\mathrm{I}_z$	"Blue-light" Irradiance at depth z
l_z	Vertical pathlength at depth z
Γ	Photo-dependent grazing constant (0.25 at day, 0.75 at night)
Z	Zooplankton abundance
k_c	Cellular carbon content of *K. brevis* ($3.6033\times10^{-3}\,mmol\,C\,cell^{-1}$)
ρ_{mean}	Mean density of seawater ($1028\,kg\,m^{-3}$)
γ	Grazing pressure coefficient

to Smagorinsky (1963), while vertical diffusivities follow the Mellor and Yamada (1982) turbulence closure scheme (Yang and Weisberg, 1999; He and Weisberg, 2003). The centered leapfrog technique was utilized with spatial gradients approximated by centered differencing, while contributions from the advective terms were obtained using a scheme developed by Easter (1993), in the manner described by Walsh et al. (2002).

Boundary conditions were established such that $\omega = 0$ at the sea surface and seafloor; at the sea surface, U and V are related to the wind stress components τ^x and τ^y by

$$\frac{K_M}{D}\left[\frac{\partial U}{\partial\sigma},\frac{\partial V}{\partial\sigma}\right] = \frac{1}{\rho_o}[\tau^x,\tau^y] \text{ as } \sigma\to 0. \tag{9}$$

At the seafloor, the horizontal velocity components are zero and vertical shear is specified by

$$\frac{K_M}{D}\left[\frac{\partial U}{\partial\sigma},\frac{\partial V}{\partial\sigma}\right] = C_Z\left[U^2+V^2\right]^{-1/2}(U,V) \text{ as } \sigma\to -1, \tag{10}$$

where

$$C_Z = MAX\left[\frac{k^2}{\left\{\ln(1+\sigma_{kb-1}H/z_o)\right\}^2},\ 0.0025\right]. \tag{11}$$

Horizontal boundary conditions over land are implemented by a land mask, which ensures that the model steps at the coast and that the normal velocity along the coastline is set to zero. The model domain has open boundaries, where depth-averaged transports normal to these boundaries are specified to be zero (Yang and Weisberg, 1999). Thus, there are no net horizontal transports into or out of the domain so the total water mass is always conserved; however, depth-dependent flows can occur into or out from the domain across open boundaries according to a Sommerfield radiation condition (Orlanski, 1976).

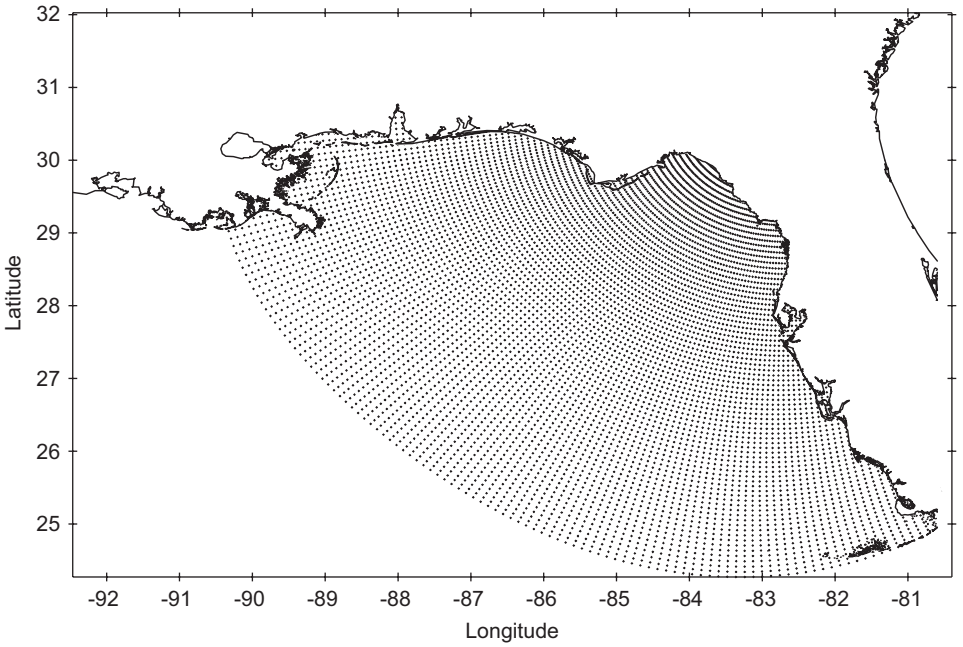

Fig. 3. The orthogonal curvilinear grid mesh of the three-dimensional coupled biophysical model of the eastern Gulf of Mexico, including the west Florida shelf.

2.3. Biological forcing

The state equation which governs phytoplankton growth (Penta, 2000; Walsh et al., 2001, 2002) is of the form

$$\frac{\partial P}{\partial t} = Tr\langle \mathrm{d}P\rangle + \mathrm{d}\langle \mu^* P\rangle - \mathrm{d}\langle eP\rangle - \mathrm{d}\langle gP\rangle - \mathrm{d}\langle lP\rangle - \frac{\partial}{\partial z}\langle wP\rangle, \quad (12)$$

where the time-dependent change in the carbon-specific *K. brevis* biomass ($\partial P/\partial t$) is defined as the advective and diffusive transport of the phytoplankton biomass ($Tr\langle \mathrm{d}P\rangle$) and the realized net growth ($\mu^* P$) thereof, less any losses due to excretion (eP), grazing (gP), cell lysis (lP), and sinking (wP), if applicable (see Table 1 for a list of the biological model parameters). Eq. (12) is coupled to the physical model using daily averages of the WFS-POM estimates of three-dimensional advection, temperature, and salinity throughout the model domain.

Since the carbon-specific losses due to phytoplankton excretion (eP) and cell lysis (lP) were assumed to be included implicitly in the calculation of the realized net growth ($\mu^* P$), Eq. 12 becomes:

$$\frac{\partial P}{\partial t} = Tr\langle \mathrm{d}P\rangle + \mathrm{d}\langle \mu^* P\rangle - \mathrm{d}\langle gP\rangle - \frac{\partial}{\partial z}\langle wP\rangle, \quad (13)$$

where the physical advective transport is defined as

$$Tr\langle \mathrm{d}B\rangle_{adv} = -\frac{1}{h_1 h_2}\begin{bmatrix} \frac{\partial}{\partial \xi}(h_2 u \mathrm{d}B) + \frac{\partial}{\partial \varsigma}(h_1 v \mathrm{d}B) \\ + h_1 h_2 \frac{\partial}{\partial \sigma}(\omega B) \end{bmatrix}, \quad (14)$$

and the diffusive transport is

$$Tr\langle \mathrm{d}B\rangle_{diff} = \frac{\partial}{\partial \sigma}\left(\frac{K_h}{d}\frac{\partial B}{\partial \sigma}\right), \quad (15)$$

where B represents any of the state variables subject to physical transport (Walsh et al., 2003).

To investigate whether maximal growth *in situ* was sufficient to yield the *K. brevis* bloom observed, phytoplankton growth was assumed to be limited by light rather than by nutrients; thus, the realized net growth rate μ^* is actually the computed light-limited (μ_L) growth rate. The temperature-dependent maximal growth rate $\mu_{(T)}$ was calculated according to Eppley (1972):

$$\mu_{(T)} = \mu_M e^{0.0633(T-27)}, \quad (16)$$

and ultimately related to the light-limited growth rate using the formulation of Steele (1962):

$$\mu^* = \mu_L = \mu_{(T)}\left(\frac{I_z}{I_{sat}}\right)e^{(1-(I_z/I_{sat}))}, \quad (17)$$

an equation which includes the effects of photoinhibition beyond the *K. brevis* saturation irradiance

I_{sat} of 55 μE m^{-2} s^{-1}, the median of the range cited by Shanley and Vargo (1993).

The time-dependent surface light field was estimated using the NCEP data of total daily (24 h) surface irradiance within the PAR wavelengths (350–700 nm), which were then interpolated as a sine function with a noon maximum and divided into discrete 360-s time steps. Irradiance at depth was determined from a variation of Beer's law:

$$I_z = I_o e^{-k_z z}, \tag{18}$$

where spectral complexity was simplified into two bands, the "red-light" and "blue-light" fractions, to allow differential attenuation of the "red" and "blue" fractions of light due to water, phytoplankton, and CDOM in a manner following the Walsh et al. (2002) model:

$$^{R}I_z = I_o \left\langle {}^{R}FRAC_I \, e^{-\int_0^z {}^{R}a_z \, dz} \left(\frac{1 - e^{-{}^{R}a_z}}{{}^{R}a_z} \right) \right\rangle, \tag{19}$$

$$^{B}I_z = I_o \left\langle {}^{B}FRAC_I \, e^{-a_c - \int_0^z {}^{B}a_z \, dz} \left(\frac{1 - e^{-a_c - {}^{B}a_z}}{a_c + {}^{B}a_z} \right) \right\rangle, \tag{20}$$

where

$$^{R,B}a_z = l_z\{{}^{R,B}a_w + (a_{chl} \bullet [\mathrm{chl}])\}. \tag{21}$$

Attenuation of blue light due to CDOM was specified based on nearshore measurements of CDOM absorption and salinity, such that salinity fields from the coupled physical model were used to determine CDOM absorption using the regression equations cited by Walsh et al. (2003). Thus, the irradiance at each depth z is simply

$$I_z = {}^{R}I_z + {}^{B}I_z. \tag{22}$$

Losses due to sinking (wP) and vertical diffusion $\partial Kz \partial P/\partial^2 z$ were tempered by the computed advection in the vertical dimension (ω) in concert with the daily vertical migration (DVM) behavior of *K. brevis*. According to Heil (1986), *K. brevis* appears to exhibit a light-triggered negative geotaxis; thus, an upward swimming velocity of 1.0 m h^{-1} was imposed when the irradiance at depth (I_z) was above zero but below saturation irradiance I_{sat}. Since *K. brevis* also exhibits a "stop response" (Baden and Mende, 1978) at light intensities of ~150 μE m^{-2} s^{-1} (Shanley, 1985), swimming direction was reversed when irradiance at depth was beyond saturation intensity (Walsh et al., 2002). At night, vertical migration velocity was set to zero.

Estimates of carbon-specific grazing losses gP were parameterized using adult copepod abundance data from oblique bongo tows at paired ECOHAB stations above the 10-m, 25-m, and 50-m isobaths during monthly cruises from August to November 1999. Differential grazing contributions as a result of zooplankton diversity were simplified by assuming only the adult copepods were capable of grazing *K. brevis* cells. Regressions of the adult copepod abundance as a function of month sampled, depth of station, and station location (e.g. along the northern or southern boundary of the ECOHAB control volume) were performed (data not shown) and applied over the entire model domain. Zooplankton abundance data from the 50-m isobath were assumed for all depths within the simulation volume greater than 50-m; likewise, data from the 10-m isobath were applied to all depths lesser than 10 m.

To investigate the maximum potential for grazing controls on red tides, the entire adult copepod population within the model was assumed to be a non-selective grazer capable of ingesting *K. brevis* cells with little apparent deleterious effects on the ingestion rate. Evidence suggests that *Acartia tonsa* is common in the coastal waters of the WFS (Lester, 2005) and is generally considered to be a non-selective grazer (Turner and Tester, 1989a), even when fed a mixed diet of toxic and non-toxic diatoms (Lincoln et al., 2001). *A. tonsa* has also been found to ingest toxic dinoflagellates as well (Jeong, 1994) and will readily feed upon *K. brevis* (Turner et al., 1998). A regression equation for the *A. tonsa* ingestion rate (as a function of *K. brevis* abundance) was previously determined by Turner and Tester (1989b) to be

$$Y = 0.8X + 129.2, \tag{23}$$

where the ingestion rate Y (10^3 cells eaten copepod^{-1} h^{-1}) is a linear function of the *K. brevis* abundance X (10^3 cells mL^{-1}). The high R^2 value for this equation (0.96) suggests that *A. tonsa* do not exhibit a saturated feeding response, even at 20,000 cells mL^{-1}, the maximum *K. brevis* concentration within the experimental range (Turner and Tester, 1989b).

Although some authors suggest that *A. tonsa* exhibits a strong DVM behavior (Fulton III, 1984; Cervetto et al., 1995), others have found *A. tonsa* to be distributed evenly throughout the water column in shallow coastal areas with only a slight trend of nocturnal migration to the surface (Stickney and

Knowles, 1975). In an effort to maximize the potential for grazing losses at all depths, *A. tonsa* was assumed to be distributed evenly throughout the photic water column. Since *A. tonsa* seems to exhibit a 2–3 fold increase in gut contents and feeding rates over the diel period (Durbin et al., 1990; Cervetto et al., 1995), periodicity of the grazing response was introduced in the form of a three-fold increase in the photo-dependent grazing constant Γ during the modeled nighttime hours (Dagg, 1995). By further incorporating the zooplankton abundance Z and an appropriate conversion factor k_c for the cellular carbon content of *K. brevis*, Eq. (23) is modified to become the term for overall grazing losses (gP), such that:

$$gP = \gamma \left\langle \left[\frac{Z \Gamma k_c}{\rho_{mean}} \right] (0.8X + 129.2) \right\rangle. \quad (24)$$

A total of four numerical experiments were performed utilizing the coupled biophysical model described herein, changing only the initial conditions within the biological model. *Case I* was initiated with a small (0.802 μmol C kg^{-1}) *K. brevis* inoculum (~33,000 cells L^{-1}) at the Sarasota 30-m isobath, just above the bottom (~29 m); *K. brevis* concentrations at all other grid points were set to zero. Grazing losses were also set to zero at all grid points throughout the course of the simulation. *Case II* was initiated with the *Case I* inoculum, but interpolated in the vertical dimension to yield a surface concentration of 0.025 μmol C kg^{-1} (~1000 cells L^{-1}). *K. brevis* concentrations at all other grid points were set to a minimal background concentration of 0.025 μmol C kg^{-1} while grazing losses remained at zero. *Case III* was performed using the initial conditions from *Case II*, but potential grazing losses were maximized using Eq. (24) and a grazing pressure coefficient γ of 1.0 to represent a grazer community electing to ingest *K. brevis* as their sole source of carbon. Within the *Case III* simulation, a refuge population of 0.025 μmol C kg^{-1} was maintained at all grid points. *Case IV* was initiated with a depth-interpolated 0.802 μmol C kg^{-1} inoculum situated just above the bottom (~29 m) at the 30-m isobath of both the Sarasota and Ft. Myers transects; *K. brevis* concentrations at all other grid points were set to zero. Grazing losses were again computed using Eq. (24), but these losses were mitigated using a grazing pressure coefficient γ of 0.005 to represent a grazer community electing to ingest *K. brevis* only 0.5% of the time. The initial conditions used in simulation *Cases I–IV* are summarized in Table 2.

Table 2
Summary of initial conditions for simulation Cases I–IV

Simulation	*K. brevis* abundance	Grazing pressure
Case I	33,000 cells L^{-1} (near bottom, Sarasota 30-m isobath only) (no depth interpolation) (no background concentrations)	None
Case II	33,000 cells L^{-1} (near bottom, Sarasota 30-m isobath only) (depth interpolation at Sarasota 30-m isobath only) (1000 cells L^{-1} throughout remaining domain)	None
Case III	33,000 cells L^{-1} (near bottom, Sarasota 30-m isobath only) (depth interpolation at Sarasota 30-m isobath only) (1000 cells L^{-1} throughout remaining domain)	Eq. (24) $\gamma = 1.0$
Case IV	33,000 cells L^{-1} (near bottom, Sarasota 30-m isobath) (near bottom, Ft. Myers 30-m isobath) (depth interpolation at 30-m isobaths) (no background concentrations)	Eq. (24) $\gamma = 0.005$

For each simulation, the propagation of the initial *K. brevis* patch was entirely dependent upon *in situ* growth, vertical migration, and sinking (as calculated by the biological model), and horizontal/vertical transport (as computed via the coupled physical model). Validation was performed utilizing data from the Mote (31 AUG 99; 12 OCT 99; 20 OCT 99), ECOHAB (07–10 SEP 99; 05–07 OCT 99; 06–07 NOV 99), and FMRI (07–14, 16–17, 20–28 SEP 99; 01, 04–08, 11–14, 18–20, 26–27 OCT 99; 02, 05–07 NOV 99) research initiatives. All model runs were conducted for 70 simulation days (30 AUG 1999–08 NOV 1999).

3. Results

3.1. Observed and modeled physical data

Acoustic Doppler Current Profilers (ADCPs) indicated that the mean monthly near-surface

currents observed during the period of bloom development were generally offshore, flowing in a northwestern direction (1.5–3.0 cm s^{-1}) in September 1999 (Fig. 4). While a near-surface convergence zone persisted near the Sarasota 15-m isobath throughout September, currents within the upper Ekman layer

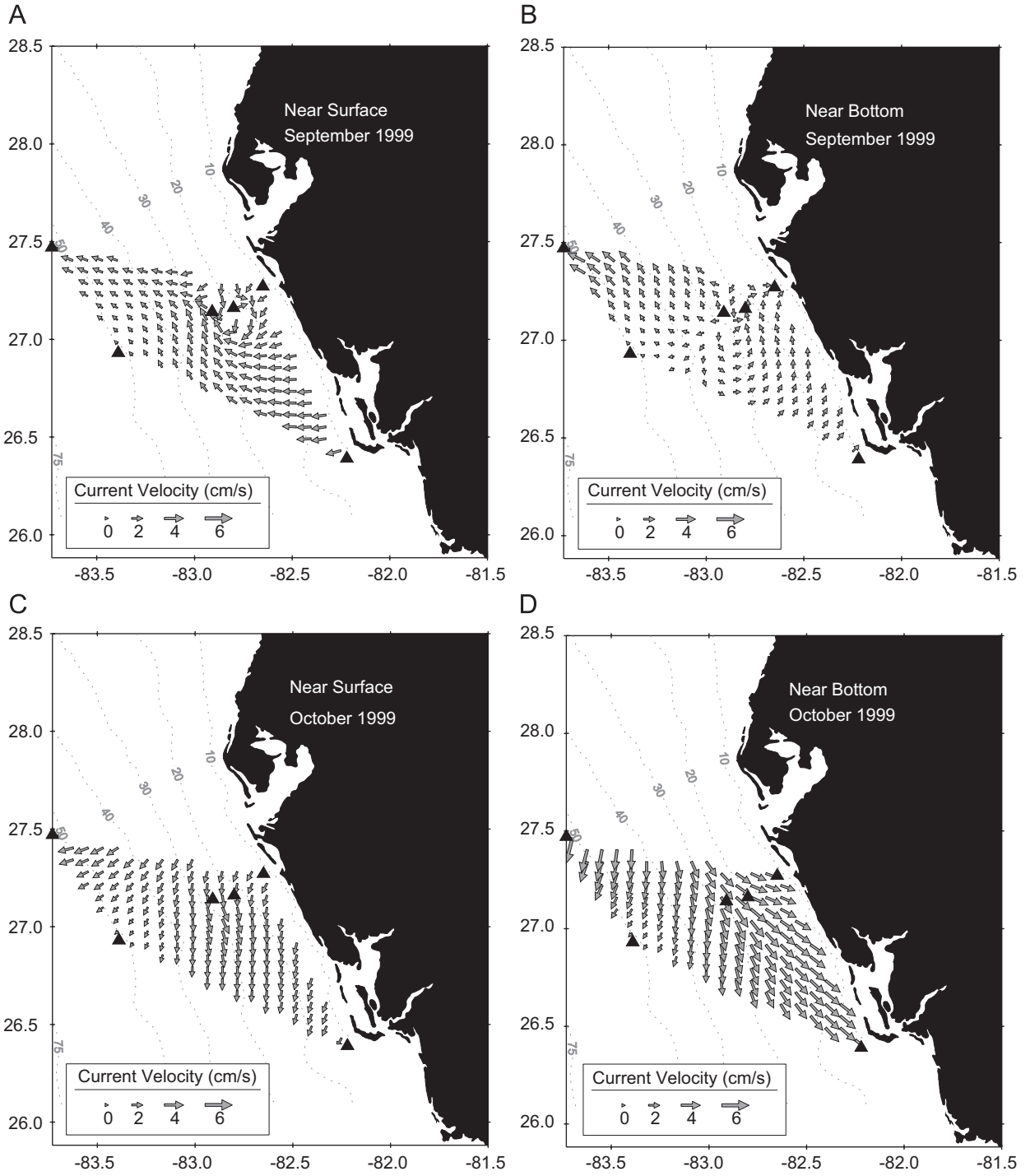

Fig. 4. Near-surface and near-bottom mean currents (cm s^{-1}) for September/October 1999 from moored acoustic Doppler current profilers (ADCPs) on the west Florida shelf.

shifted to the south (1.7–3.8 cm s^{-1}) in October. In contrast, the near-bottom currents at nearshore moorings were oriented in a north to northeast direction in September (1.7–3.8 cm s^{-1}), and relative to the geometry of the west Florida coast, were slightly onshore. By October, the mean near-bottom currents had increased in magnitude (2.6–6.0 cm s^{-1}) and had shifted to an alongshore flow to the southeast. The east (***u***) and north (***v***) vector components of the modeled currents along the Tampa, Sarasota, and Fort Meyers transect lines during the month of bloom development (Fig. 5) indicate that the temporal- and depth-dependent variability of the simulated flowfields are consistent with the stratified flows observed at inner-shelf ADCP moorings, indicating onshore flow in the bottom Ekman layer and an offshore flow at the surface.

3.2. Observed and modeled ecological data

During surface and near-bottom sampling for *K. brevis* along the Mote red tide stations on 31 August 1999, the only *K. brevis* detected was a small amount of *K. brevis* (33,000 cells L^{-1}) located approximately 46 km offshore, just above the bottom at the Sarasota 30-m isobath. Two weeks later, ECOHAB, Mote, and FMRI stations indicated the presence of several distinct patches at the surface, the largest of which (151,000 cells L^{-1}) was located just outside the mouth of Charlotte Harbor (Fig. 1). By early October, the large red tide (5.9×10^6 cells L^{-1}) was confined along the coast between Tampa Bay and Charlotte Harbor. By 20 October 1999, very little *K. brevis* (12,000 cells L^{-1}) remained off the coast of Sarasota, and by early November, the red tide had been completely eliminated. Concurrent zooplankton sampling during ECOHAB cruises indicated that zooplankton abundance at nearshore stations decreased throughout the duration of the red tide, such that the maximal zooplankton abundance of 14,600 ind. m^{-3} was reduced to 4824 ind. m^{-3} from September to November.

Depth profiles of chlorophyll-*a*, DIN, DIP, and silicate were also determined from ECOHAB cruises along the Sarasota (Fig. 6) and Ft. Myers (Fig. 7) transects throughout the period of red tide development. Prior to October 1999, Sarasota algal stocks were <2.45 μg chl-*a* L^{-1} at the 10-m isobath (Fig. 6(A1)). DIN, DIP, and silicate profiles (Figs. 6(C1)–(E1)) indicated that these waters were nitrogen poor (with a DIN:DIP ratio of ~1–2). By October 7th, chlorophyll maximum at the 10-m isobath had grown to 19.12 μg chl-*a* L^{-1} (Figs. 6(A2)), despite persistent inorganic nitrogen limitation (Figs. 6(C2) and (D2)). Within a month, algal stocks returned to ~2.34 μg chl-*a* L^{-1} at the 10-m isobath, while *K. brevis* had returned to $<1{,}000$ cells L^{-1} (Figs. 6(A3) and (B3)). Despite a fivefold reduction in DIP and a tenfold reduction in silicate during this period, inorganic nitrogen was still limiting (Figs. 6(C3)–(E3)).

Although the algal (<2.4 μg chl-*a* L^{-1}) and silicate (<15 μmol Si kg^{-1}) stocks at the Ft. Myers 10-m isobath were similar in magnitude to those observed offshore Sarasota in September (Figs. 7(A1) and (E1)), DIN (<0.39 μmol N kg^{-1})and DIP (<0.52 μmol P kg^{-1}) concentrations were slightly higher (Figs. 7(C1) and (D1)). While a small amount of *K. brevis* (2000 cells L^{-1}) was observed at the surface of the 30-m isobath in September (Fig. 7(B1)), only 7500 cells L^{-1} were observed at the 10-m isobath on October 6th (Fig. 7(B2)), despite the large red tide (5.9×10^6 cells L^{-1}) measured along Englewood Beach, some 83 km to the north (Fig. 1(B)). Silicate and DIP stocks were reduced two- to threefold during this period, as the regions of maximal DIN, DIP, and silica concentrations shifted 10–30 km offshore (Figs. 7(C2)–(E2)). By November, *K. brevis* had returned to background concentrations, while a localized region of maximal DIN concentration (1.06 μmol N kg^{-1}) persisted near the bottom approximately 10 km offshore (Figs. 7(B3) and (C3)).

Case I simulation results indicate a small (1000 cells L^{-1}) surface population of *K. brevis* at the Sarasota 30-m isobath (Fig. 8(A)). By October 8th, the *Case I* simulation indicated that the center of maximum surface concentrations of *K. brevis* (12,000 cells L^{-1}) had traveled northwest to the 40-m isobath of the Tampa transect (Fig. 8(B)). The model failed to predict the large red tide (5.9×10^6 cells L^{-1}) observed along the coast between Tampa Bay and Charlotte Harbor, nor were any of the predicted *K. brevis* cells observed at the surface along the Tampa transect during the October 4–8 ECOHAB cruise (Fig. 1(B)).

While the *Case II* simulation was successful in reproducing the magnitude of *K. brevis* concentrations sampled at the Sarasota 10-m isobath (1.9×10^6 cells L^{-1}) by October 4–8 (Fig. 8(D)), there was little resemblance to the observed spatial fields of *K. brevis* at the surface throughout the

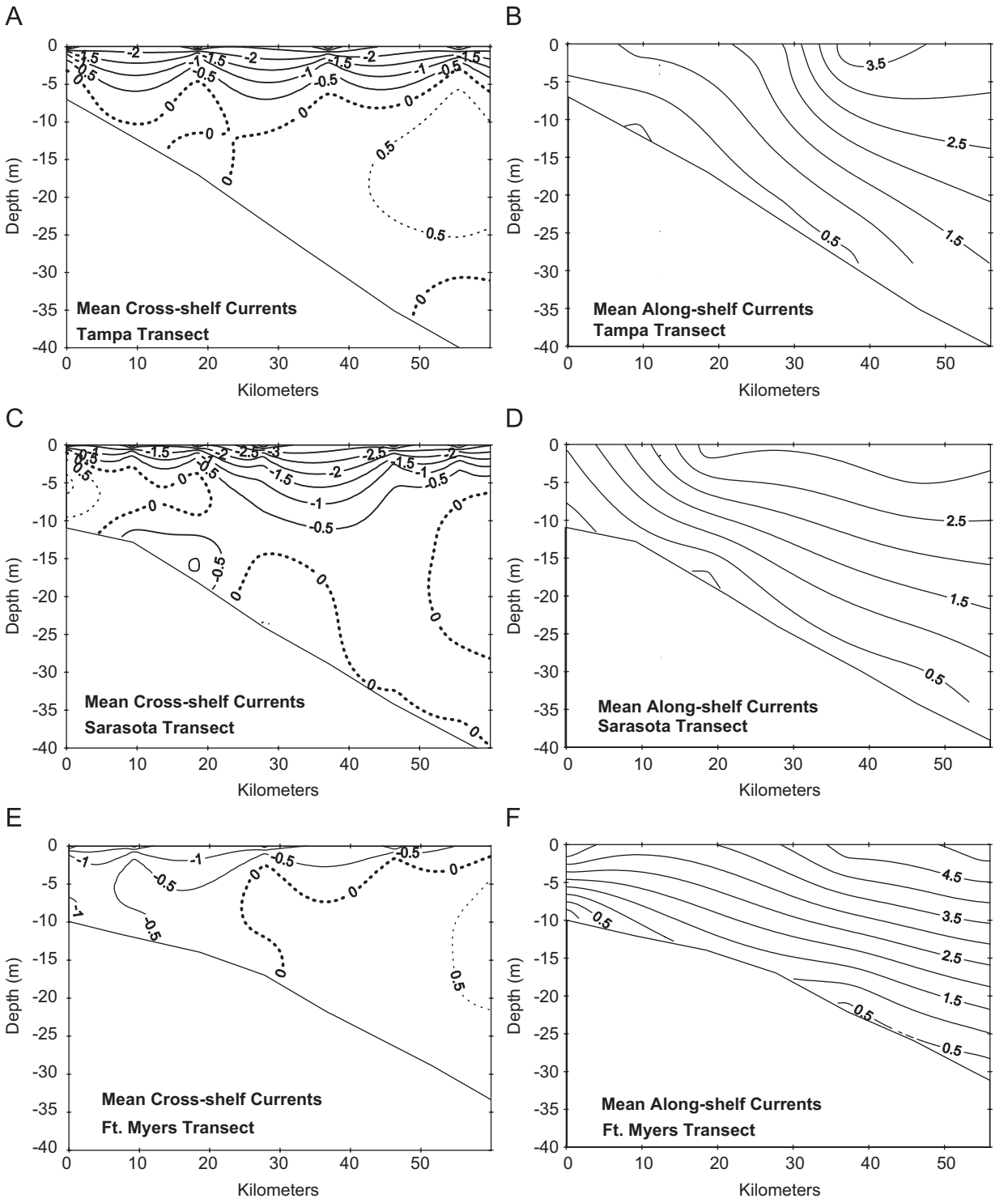

Fig. 5. Modeled estimates of the average daily cross- (***u***) and along-shelf (***v***) transport relative to the Tampa (A, B), Sarasota (C, D), and Ft. Myers (E, F) transects during the month of bloom development. Solid lines indicate flow offshore or alongshore to the north. Broken lines indicate flow onshore or alongshore to the south. Contours represent 0.5 cm s^{-1} current velocity.

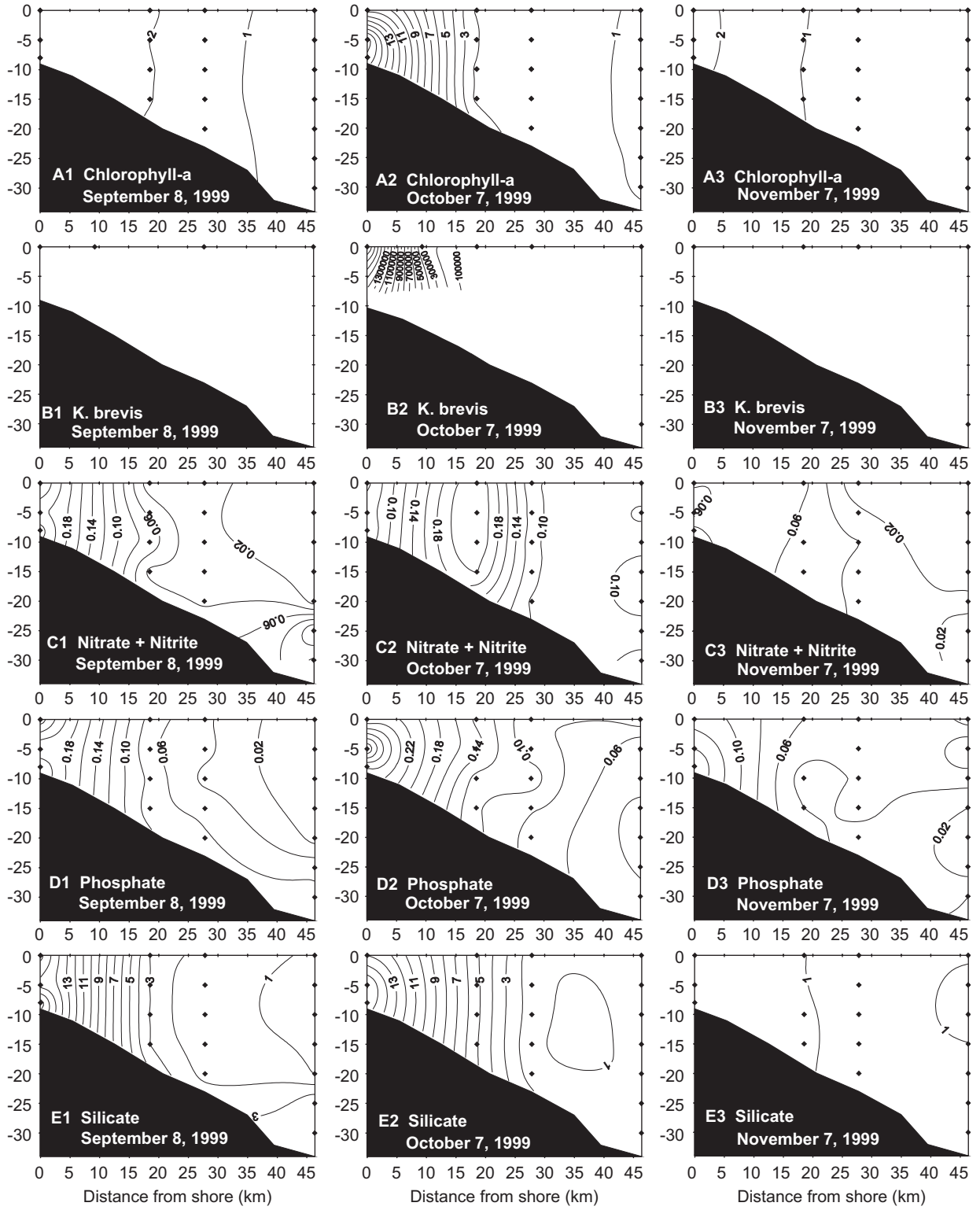

Fig. 6. Depth profiles of (A) chlorophyll-*a* ($\mu g\,L^{-1}$); (B) *K. brevis* (cells L^{-1}); (C) dissolved inorganic nitrogen (μM); (D) dissolved inorganic phosphorus (μM); and (E) dissolved silicate (μM) on (1) 08 September; (2) 07 October; and (3) 07 November 1999 above the 30-m isobath of the Sarasota transect.

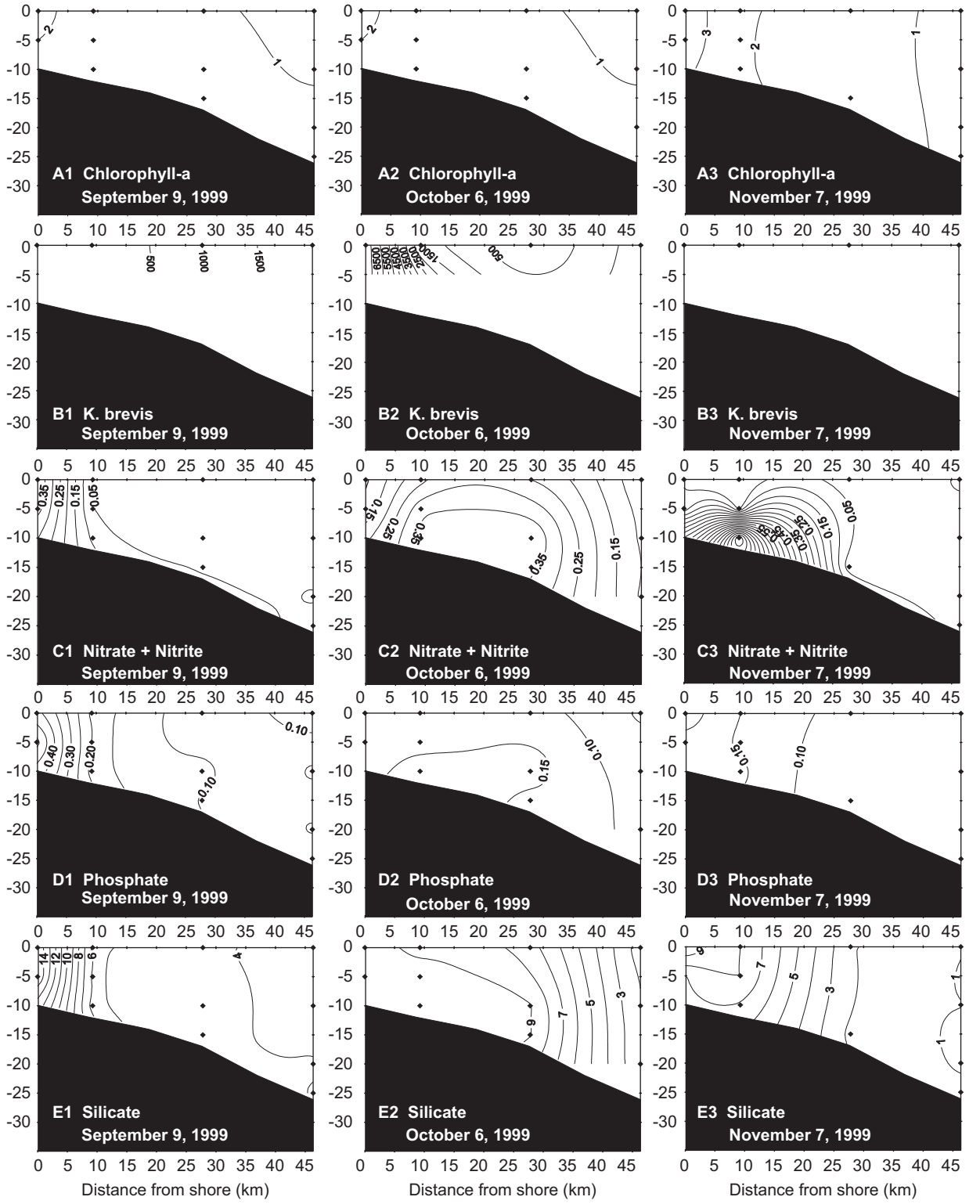

Fig. 7. Depth profiles of (A) chlorophyll-*a* ($\mu g\,L^{-1}$); (B) *K. brevis* (cells L^{-1}); (C) dissolved inorganic nitrogen (μM); (D) dissolved inorganic phosphorus (μM); and E) dissolved silicate (μM) on (1) 08 September; (2) 07 October; and (3) 07 November 1999 above the 30-m isobath of the Fort Myers transect.

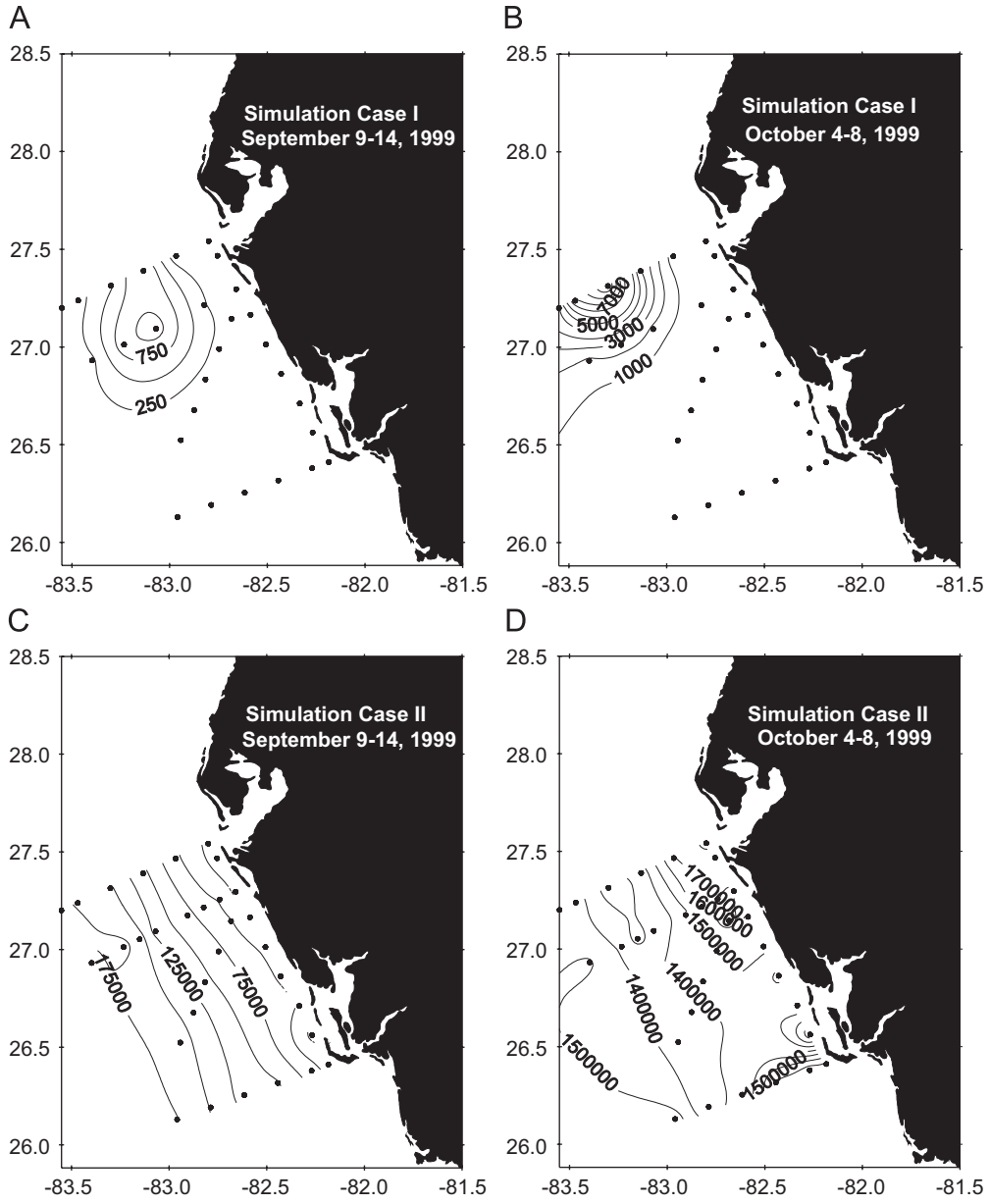

Fig. 8. Modeled surface concentrations of *K. brevis* (cells L^{-1}) for simulation: (A) *Case I*, September 09–14; (B) *Case I*, October 04–08; (C) *Case II*, September 09–14; and (D) *Case II*, October 04–08, 1999.

simulation period (Fig. 1(A) and (B)). Furthermore, the model predicted offshore maxima of *K. brevis* abundance on September 9–14 (Fig. 8(C)) and October 4–8 (Fig. 8(D)), contrary to the observed fields.

Similar to *Case II*, the *Case III* simulation failed to predict the spatial fields of *K. brevis* observed at the surface for either period of September 9–14 (Figs. 5(A) and 9(A)) or October 4–8 (Figs. 5(B) and 9(B)). However, the addition of maximum grazing pressure in the *Case III* simulation significantly mitigated net algal growth, relative to *Case II*.

The spatial fields of *K. brevis* observed from September 9–14 (Fig. 1(A)) were generally in keeping with *Case IV* predictions, although both the magnitude and displacement offshore of the surface *K. brevis* were over estimated by the model

(Fig. 9(C)). Although the model significantly under estimated the magnitude of the October 4–8 red tide (Fig. 9(D)), the bimodal character of the observed red tide (Fig. 1(B)) was successfully predicted despite its displacement ~40 km offshore. None of the simulations predicted the swift decline of the red tide, whereas *K. brevis* was completely absent from west Florida coast waters by November 5th (Figs. 1(C) and (D)).

4. Discussion

4.1. Analysis of observed and modeled physical data

Comparisons made between observed velocity vectors at moored ADCPs and those simulated by the physical model indicate that in addition to sea level, the observed currents compare reasonably well to those computed by the WFS-POM (He and

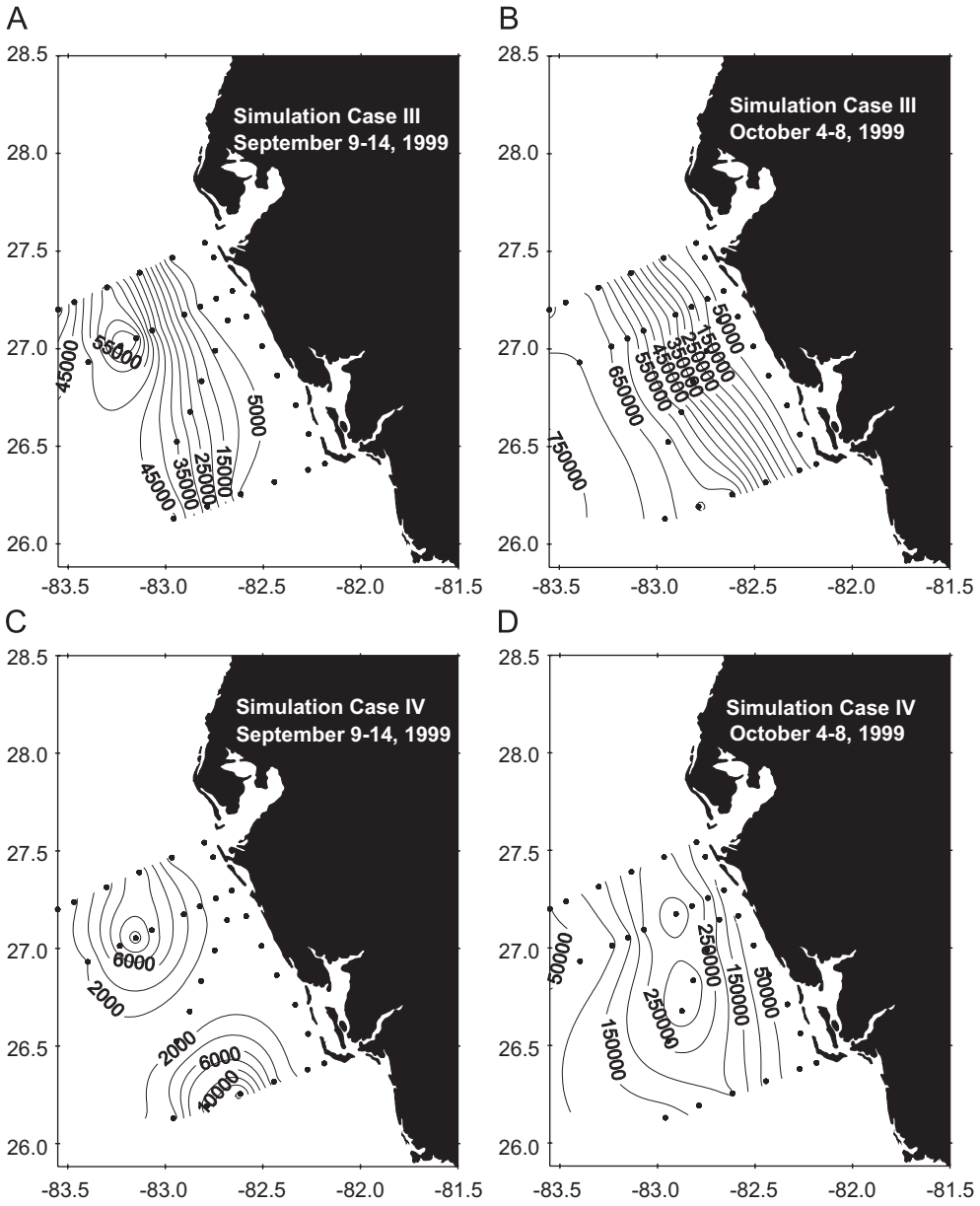

Fig. 9. Modeled surface concentrations of *K. brevis* (cells L^{-1}) for simulation: (A) *Case III*, September 09–14; (B) *Case III*, October 04–08; (C) *Case IV*, September 09–14; and (D) *Case IV*, October 04–08, 1999.

Weisberg, 2003). While previous analyses of the WFS-POM have found that the model occasionally fails to replicate reversals in the observed currents, the model does capture the general features of the observations, especially the sense of rotation in both the surface and bottom Ekman layers (He and Weisberg, 2003).

Local forcing largely controls the inner-shelf circulation, particularly with respect to the coastline and isobath geometries relative to the seasonal wind patterns (He and Weisberg, 2003). Because of these unique geometries, the region offshore and between Tampa Bay and Charlotte Harbor is often the site of flow field confluence in the bottom Ekman layer, resulting in an augmentation of upwelling (Weisberg et al., 2000). Periods of significant stratification (i.e. during the summer to fall transition) can also lead to an increase in the magnitude of the upwelling response, which tends to be more spatially confined near the coast as a result (Weisberg et al., 2000). Indeed, this upwelling favorable circulation pattern appears to be a common feature on the WFS during the fall season (He and Weisberg, 2003).

A review of the modeled flowfields offshore Sarasota and Fort Myers indicate that a strong northern ($\boldsymbol{v}+$) and even a weak western ($\boldsymbol{u}-$) component of the overall current vector would result in a nearshore shoaling of the bottom Ekman layer, given the "downstream" orientation of the west Florida coastline relative to the vector components of flow. Offshore Fort Myers, the near-bottom western component ($\boldsymbol{u}$) of the current velocity was positive to the 20-m isobath (35 km offshore), while the northern component ($\boldsymbol{v}$) was approximately $1.0\,\mathrm{cm\,s^{-1}}$, or $\sim 0.86\,\mathrm{km\,day^{-1}}$ (Figs. 5(E) and (F)). Near-bottom currents at the Sarasota 30-m isobath were also slightly onshore (Figs. 5(C) and (D)). Thus, the transport of materials from the mid-shelf to the coast could only have been facilitated by the net onshore flow of sub-surface layers beyond the Sarasota and Fort Myers 20-m isobaths, provided that those materials were confined near the bottom.

Separate from this mid-shelf transport paradigm, moored ADCPs indicated that the near-bottom currents inshore of the Sarasota and Fort Myers 10-m isobaths were slightly onshore throughout September (Fig. 4(B)). Since the alongshore component of velocity near the bottom was effectively zero (Fig. 5), any materials within the sub-surface layers inshore of the 10-m isobath would be slowly transported directly inshore (eastward).

If the red tide found near Sarasota on 04–08 October 1999 (Fig. 1(B)) was the result of the maintenance and transport of the near-bottom inoculum that was sampled ~46 km offshore some 37 days earlier, the average daily cross-shelf transport of the developing red tide must have exceeded $1.25\,\mathrm{km\,day^{-1}}$, or $1.45\,\mathrm{cm\,s^{-1}}$. Although ADCP data throughout September 1999 indicate that the near-bottom currents were weakly onshore (Fig. 4(B)), model estimates of the cross-shelf transport along the Sarasota line (Fig. 5(C)) indicate that during the presumed month of bloom development, onshore cross-shelf transport rates in the bottom Ekman layer never exceeded $0.55\,\mathrm{cm\,s^{-1}}$. Regardless of the modeled flowfields, the ADCP sensor moored at the 30 m isobath measured a mean monthly cross-shelf transport along the Sarasota line of $0.94\,\mathrm{cm\,s^{-1}}$ ($\sim 0.81\,\mathrm{km\,day^{-1}}$) in the bottom Ekman layer throughout September 1999 (Fig. 4(B)). While this would have transported the 31 August 1999 inoculum ~30 km inshore by 05 October 1999 (to within 16 km of the coast), this would only be possible if the developing red tide remained in the near-bottom Ekman layer throughout the entire transit inshore.

Throughout October, the near-bottom currents were oriented alongshore to the southeast, although the geometry of the coast would still result in the onshore transport of materials contained within the bottom Ekman layer, especially at locations inshore of the 30-m isobath (Fig. 4(D)). However, any materials confined to the surface Ekman layer would have been swiftly transported offshore and out of the ECOHAB control volume from September to October (Figs. 4(A) and 5(C)).

4.2. Analysis of observed ecological data

In order for red tides to occur on the WFS, especially those of the magnitude ($5.9 \times 10^6\,\mathrm{cells\,L^{-1}}$) witnessed from October 4 to 8 offshore Englewood Beach (Fig. 1(B)), a sufficient source of nitrogen is required, particularly at the coast where the greatest concentrations of *K. brevis* were observed. Indeed, inorganic nitrogen stocks (nitrate + nitrite) were indicative of estuarine sourcing and decreased to only 0.05–0.15 μM N within 10 km of the coast throughout September 1999 (Figs. 6(C)1 and 7(C)1). Since the observed red tide would have required ~22 μM N, assuming Redfield proportions and a cellular carbon content of $300\,\mathrm{pg\,C\,cell^{-1}}$ (Walsh et al., 2001), *K. brevis* must have harvested its required

nitrogen from other sources. This is a particularly important point since the ecological simulations assumed that *K. brevis* were not nutrient limited.

This alternate source of nitrogen was assumed to be the result of an aeolian iron loading event, resulting in the stimulation of nitrogen fixation by the diazotroph *Trichodesmium*, which in turn led to an increase in DON in WFS waters. In fact, Lenes et al. (2001) have shown that the October 1999 red tide was preceded by a period of increased atmospheric deposition of iron and that the *in situ* DON stocks (Fig. 10(B1)) were indeed sufficient to fuel the nitrogen demands of the developing red tide, assuming the DON stocks were labile. Of course, a sufficient source of phosphorus is also necessary to maintain balanced growth. With a maximum phosphorus requirement of ~1.4 μM P, the large red tide developing between two estuarine sources of phosphorus (Tampa Bay and Charlotte Harbor) would benefit from the high concentrations of *in situ* DIP (up to 0.5 μM) supplied to coastal waters by these two estuarine systems (Fig. 10(C1)).

A red tide developing in proximity to an estuarine source of DIP would also benefit from the protective UV umbrella of the associated outfall of CDOM. In shallow water, a *K. brevis* patch at or near the surface would be incapable of migrating downward to a depth sufficient to avoid UV damage and/or photo-inhibitory effects (Walsh et al., 2002). Thus, the increased spectral absorption of light due to CDOM at the surface could prevent photo-inhibition and/or UV-induced cell lysis, effectively shading a fledgling bloom of *K. brevis*. In deeper water, the shade-adapted *K. brevis* cells would be capable of retreating to a depth where $I_z \rightarrow I_{sat}$, thereby providing a mechanism through which *K. brevis* could maintain position in the bottom Ekman layer.

While a complementary proto- and metazoan grazer community that serves to eliminate all potential phytoplankton competitors would ultimately grant refuge to the more unpalatable cells of *K. brevis*, these grazers would have to exhibit some degree of prey selection/avoidance in order to provide a selective advantage to *K. brevis*. Since zooplankton abundance is often maximal nearshore (Fig. 1), the dominance of selective grazers in these waters would place increased grazing pressure on phytoplankton competitors while providing some degree of grazing refuge to *K. brevis*. Without invoking paradigms of phytoplankton competition, it was necessary to first determine if a grazer community could mitigate or eliminate a red tide merely as a consequence of *K. brevis* ingestion.

4.3. Analysis of modeled ecological data: Case I

Blooms of *K. brevis* have long been purported to originate 18–74 km offshore (Steidinger, 1973, 1975, Steidinger and Haddad, 1981), preferring salinities of more oceanic (32-35 ppt) than estuarine influence (Wilson, 1967). Thus, if *K. brevis* is indeed an oceanic species, any red tide observed at the coast would necessarily require a paradigm of offshore initiation and subsequent transport to nearshore waters. During the weeks preceding the October 1999 red tide, the near-bottom currents of the mid-shelf were onshore (Fig. 5). Since *K. brevis* is a shade-adapted organism, a near-bottom inoculum maintaining its position in the bottom Ekman layer would ultimately be transported onshore. However, model results indicate that the depth of optimal light utilization was at ~20 m, nearly 10 m above the bottom. With a migration velocity of $1.0\,m\,h^{-1}$, the light-cued ascent behavior of *K. brevis* caused the inoculum to become displaced from the bottom Ekman layer within a day. By October 4th, instead of seeding the red tide observed at the coast, the inoculum had been advected offshore, exiting the ECOHAB control volume to the northwest (Fig. 8(B)). Therefore, the October 1999 red tide observed along the coast between Sarasota and Fort Myers could not possibly have been initiated by the sub-surface inoculum as a sole consequence of advection under *Case I* conditions.

4.4. Analysis of modeled ecological data: Case II

While the *Case II* simulation was initialized with a depth-interpolated inoculum at the Sarasota 30-m isobath, the model also assumed that the entire ECOHAB control volume was homogenously populated with *K. brevis* at a background concentration of $1000\,cells\,L^{-1}$ with no grazing pressure applied, regardless of cell concentrations. Although this simulation predicted larger offshore concentrations of *K. brevis* than were observed by September 9th (Fig. 8(C)), the simulation was capable of replicating the nearshore maxima of *K. brevis* observed on October 4–8 (Figs. 1(B) and 8(D)). These model results suggest that even a small (but ubiquitous) background concentration of *K. brevis* near the coast would have been capable

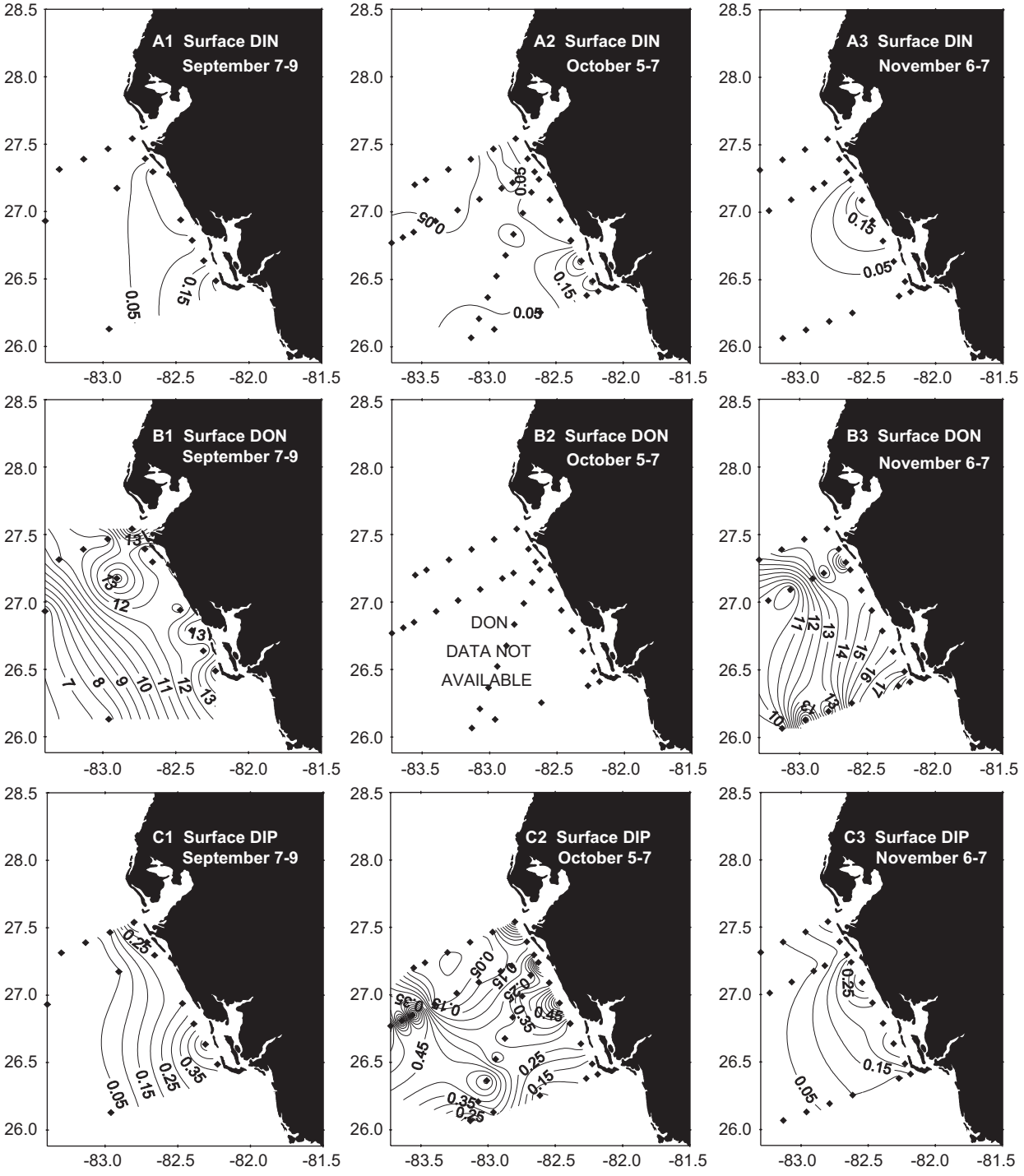

Fig. 10. Surface stocks of (A) dissolved inorganic nitrogen (μM); (B) dissolved organic nitrogen (μM); and (C) dissolved inorganic phosphorus (μM) from (1) September 07–09; (2) October 05–07; and (3) November 06–07, 1999.

of maintaining position near the coast, growing to a red tide of $\sim 1.8 \times 10^6$ cells L^{-1}, assuming a complete lack of grazing pressure. These model results also presume that the red tide was not limited by nutrient availability. While the observed TDN and TDP stocks available to nearshore *K. brevis* may not have

become limiting until the red tide reached $\sim 2.3 \times 10^6$ cells L^{-1} (Figs. 10(A1)–(C1)), this assumption was not applicable to the offshore concentrations of *K. brevis*. Hence, the imposition of nutrient limitation in the oligotrophic waters offshore may have resulted in shelf-wide *K. brevis* fields more similar to those observed on October 4–8 (Fig. 1(B)).

This scenario assumes that background populations of *K. brevis* were growing steadily along the coast between Sarasota and Fort Myers for the entire period preceding the October red tide; however, this pattern was not observed. In fact, the nearshore surface stocks of *K. brevis* were only slightly above ($\sim$2500 cells L^{-1}) the simulated background concentrations by September 9th, with the exception of a larger patch (151,000 cells L^{-1}) that appeared near the coast offshore Ft. Myers (Fig. 1(A)). Thus, it was unlikely that the steady growth of the background populations of *K. brevis* near the coast throughout September could fully explain the dynamics of the large red tide observed there a month later.

4.5. Analysis of modeled ecological data: Case III

Case III conditions were identical to those in *Case II* except for the imposition of maximal grazing losses to represent a grazer community feeding solely on *K. brevis* cells. By September 9th, the modeled *K. brevis* stocks were reduced three- to fivefold from the *Case II* simulation (Figs. 8(C) and 9(A)), resulting in an offshore maximum due to high zooplankton abundance in nearshore waters (Fig. 1(A)). By October 4–8, nearshore *K. brevis* stocks were reduced by a factor of 36 compared to those computed during the *Case II* simulation (Figs. 8(D)). Although the *Case III* simulations (Fig. 9(A) and (B)) did not resemble the observed fields of *K. brevis* (Figs. 1(A) and (B)), the simulation predicts that background populations of *K. brevis*, under conditions of maximal growth, could consistently produce more algal biomass than was capable of being grazed.

4.6. Analysis of modeled ecological data: Case IV

Although a near-bottom inoculum was sampled only at the Sarasota 30-m isobath on August 31st, the simulated flowfields indicated that a weak onshore flow of the bottom Ekman layer was also present at the mid-shelf near Fort Myers (Fig. 5(E)). Since there was evidence of a *K. brevis* inoculum offshore Fort Myers in early September as well (Fig. 1(A)), the *Case IV* simulation was initialized with a presumed near-bottom inoculum at the Fort Myers 30-m isobath in an attempt to test the paradigm of near-bottom onshore transport along both the Sarasota and Fort Myers transects. The removal of all background populations of *K. brevis* and an imposition of a more realistic ($\gamma = 0.005$) grazing pressure (Walsh et al., 2003) yielded model results from September 9–14 and October 4 to 8 (Figs. 9(C) and (D)) that better reflected the spatial character of the observed *K. brevis* fields (Figs. 1(A) and (B)).

From October 4 to 8, the modeled red tide was located along the 20-m isobath, with *K. brevis* distributed unevenly throughout the entire water column ($\sim$300,000 cells L^{-1} mean concentration). However, if the sum of *K. brevis* throughout the entire water column were concentrated within a layer approximately 3-m thick and located near the surface, the aggregated red tide would be $\sim 2.1 \times 10^6$ cells L^{-1}. Although phytoplankton biomass has been shown to accumulate along density fronts (Margalef et al., 1979; Taft and Martin, 1986; Fraga et al., 1990; Franks, 1992), such fronts would tend to aggregate phytoplankton at depth near the pycnocline, not at the surface. To concentrate *K. brevis* at the surface, a shading paradigm must be invoked as an alternate aggregational mechanism.

During instances of shading, most phytoplankton compensate by modifying the content and composition of the pigment suite as a long-term response to light limitation (Kirk, 1994); however, the short-term response of *K. brevis* to such incidents would be an ascent to (and aggregation within) a layer where $I_z \rightarrow I_{sat}$. While most shading paradigms commonly utilize cloud cover and/or estuarine sources of CDOM to reduce available light, large phytoplankton blooms at the surface can also be quite effective in reducing I_z. As *K. brevis* chlorophyll concentrations increase, so too does the attenuation of light (Eq. (18)), resulting in a shoaling of the optimal light climate. Model simulations of the coefficient of light limitation ($\mu_L \mu_{(T)}^{-1}$) indicate that the initial depth of optimal light intensity is from 15 to 30 m (Fig. 11). Since the *Case II* stocks of *K. brevis* were the highest of all the simulations, the depth of optimal light intensity had been shoaled to 12–22 m by September 14th and as shallow as 4–7 m by October 4th (Fig. 11A). In contrast, the lower concentrations of *K. brevis* in the

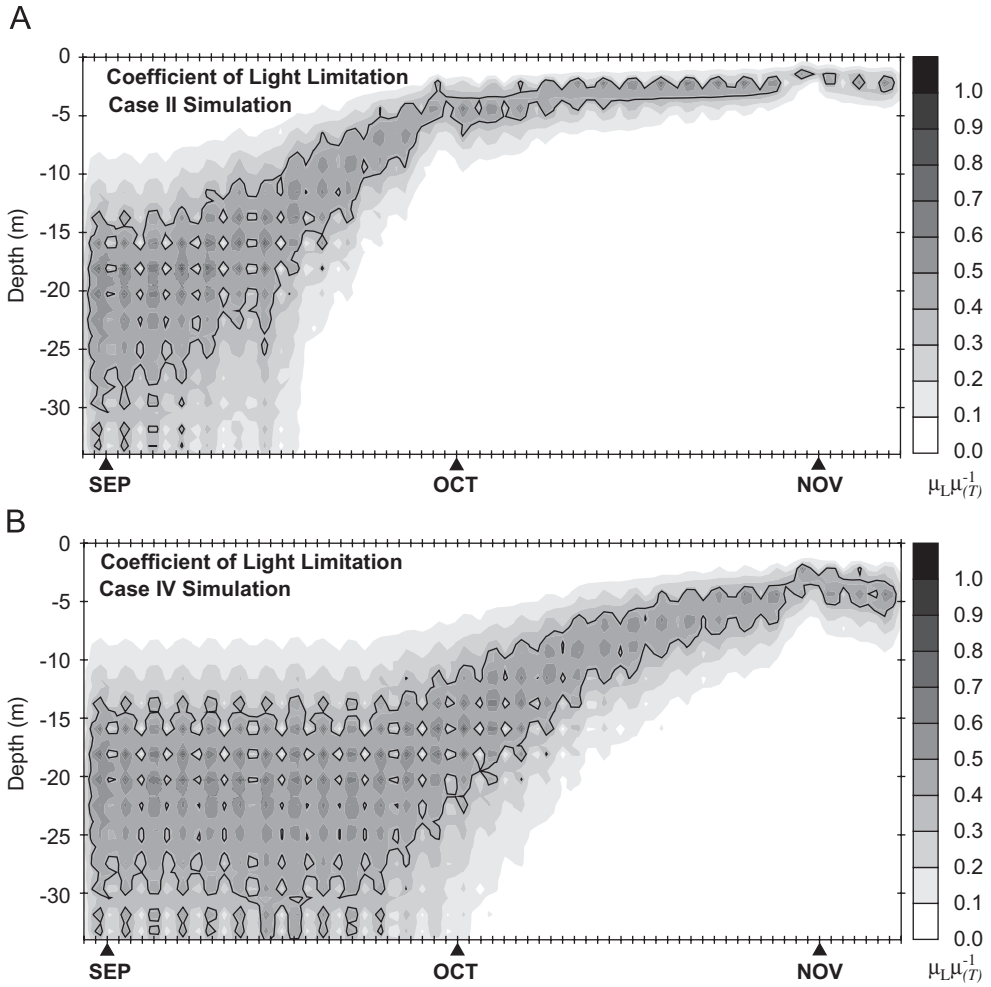

Fig. 11. Modeled coefficient of light limitation ($\mu_L\mu_{(T)}^{-1}$) above the 30-m isobath of the Sarasota transect from 30 August to 08 November 1999. Solid line indicates the depth range at which the realized net growth rate (μ^*) of *K. brevis* was $\geqslant 0.3\,\text{day}^{-1}$.

Case IV simulation maintained the depth of optimal light intensity at 15–30 m through September 14th but had shoaled to 10–17 m by October 4th (Fig. 11(B)).

Modeled data from all cases indicates that self-shading does not seem to affect the depth of optimal light intensity, provided that mean *K. brevis* concentrations are below 100,000 cells L^{-1} (Fig. 12). Beyond this threshold, self-shading begins to affect light intensity at depth, effectively narrowing the depth range of I_{sat} and driving it higher in the water column. In an attempt to maximize light interception in a region where $I_z \approx I_{sat}$, the light-cued ascent behavior of *K. brevis* would tend to concentrate cells within this narrowing depth range of optimal light, which in turn would further increase the magnitude of this self-shading paradigm. This aggregational mechanism could potentially lead to a "shade-induced" red tide concentrated near the surface, as suggested by the *Case II* simulation (Fig. 11(A)).

Of course, any shade-induced red tide would necessarily occupy the surface Ekman layer; in the context of these simulations, this would result in the swift transport of the bloom offshore, given the surface flowfields observed from September to October 1999 (Figs. 4 and 5). However, the onshore transport of a red tide would also decrease the overall depth of the water column, effectively increasing the maximum I_z just above the bottom. If the shoaling of the bottom Ekman layer was complimentary to the shoaling of the coefficient of light limitation ($\mu_L\mu_{(T)}^{-1}$) during onshore transport, a self-shaded red tide could continue to grow while

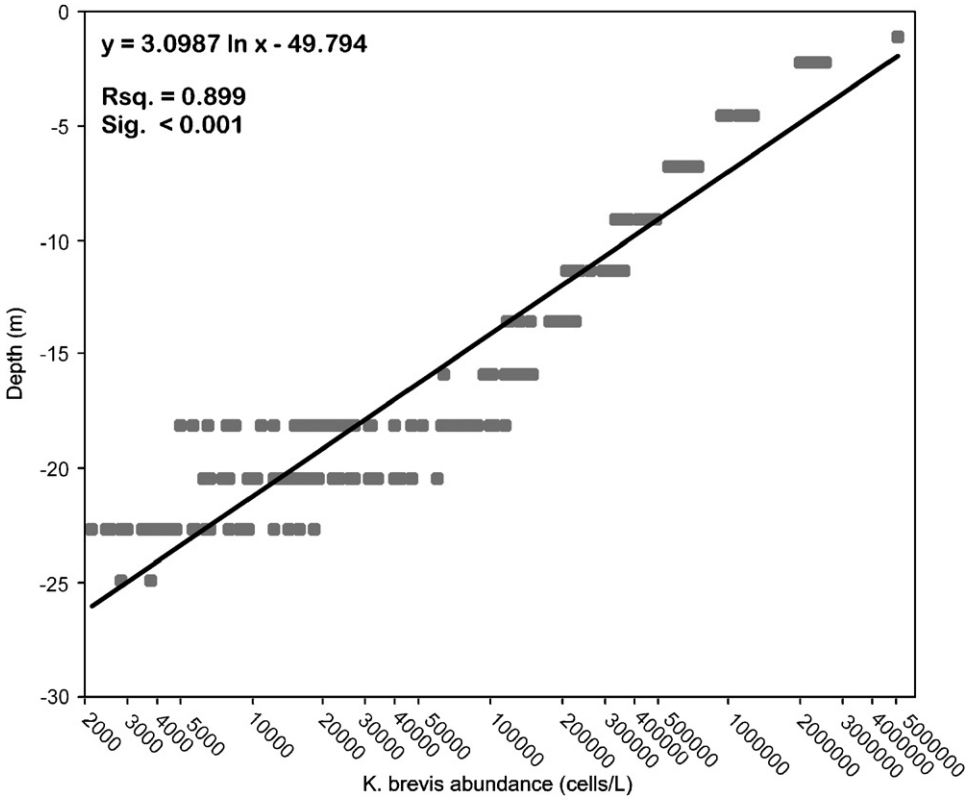

Fig. 12. Modeled relationship between *K. brevis* abundance (cells L^{-1}) and their required position in the water column where $\mu_L \approx \mu_{(T)}$. Solid line indicates the theoretical depth at which *K. brevis* may avoid light limitation as a consequence of self-shading.

maintaining position in the bottom Ekman layer during periods of coastal upwelling.

4.7. Analysis of modeled ecological data: general observations and conclusions

None of the numerical experiments were able to replicate the observed *K. brevis* fields from September to October 1999, suggesting that a more complex grazing and/or light scheme and an explicit calculation of nutrient limitation relative to other phytoplankton competitors will be necessary to fully describe the fundamental elements of red tide maintenance. Despite the simplicity of the biological model utilized in this study, a number of features critical to the dynamics of the October 1999 red tide were tested successfully, enabling the following conclusions to be made:

(1) The measured and modeled flowfields were insufficient in both direction and magnitude to fully deliver the 31 August 1999 near-bottom inoculum to the coast, thus contradicting the assertion that the red tide observed between Sarasota and Charlotte Harbor during 04–08 October 1999 was caused solely by the offshore maintenance of *K. brevis* in the bottom Ekman layer which was ultimately delivered to the coast as a result of upwelling (*Case I*).

(2) Background concentrations ($\sim$1000 cells L^{-1}) of *K. brevis* could indeed grow into a red tide of over 2×10^6 cells L^{-1} in place near the coast in the 37-day period of bloom development, assuming estuarine initiation with no nutrient limitation, no grazing losses, and no competition from other phytoplankton species (*Case II*).

(3) Maximal grazing pressure could not prevent the development of a red tide or cause its termination once initiated at 33,000 cells L^{-1}, even when *K. brevis* was the sole species of phytoplankton grazed. Assuming no other losses to algal biomass and a zooplankton community ingestion rate similar to that of *A. tonsa*, the grazer community could only limit the extent or delay the development of a significant red tide (*Case III*).

(4) Mean *K. brevis* concentrations in excess of $\sim$100,000 cells L^{-1} generally result in significant self-shading, thereby reducing the depth of the I_{sat} ($55\,\mu E\,m^{-2}\,s^{-1}$) isolume. The light-cued ascent behavior of *K. brevis* would thus result in a concentration of *K. brevis* cells at or near the I_{sat} isolume, indicating the possibility of a "shade-induced" aggregational mechanism which contributes to the frequency of significant red tides in shallow coastal waters (*Case IV*).

Of course, further refinements to the biological model will be necessary to fully describe the dynamics of this red tide event along the WFS. Improvements in model fidelity will be accomplished in the future by the inclusion of: phytoplankton competitors; an explicit calculation of nutrient availability and limitation; a more realistic rendering of the spectral light field and the attendant effects of photo-inhibition/compensation; and a mixed community of vertically migrating proto- and metazoan grazers. These model refinements are currently under development and shall be used to aid progress toward an operational model of red tide forecasting along the WFS.

Acknowledgments

This analysis was funded by Grants NA76RG0463 and NA96OP0084 from the National Oceanic and Atmospheric Administration to JJW, GAV, and RHW, R827085-01-0 from the Environmental Protection Agency to GAV and NAG5-6449 to JJW from the National Aeronautics and Space Administration, 1435-0001-30804 to RHW, as well as N00014-99-1-0212 to JJW and N00014-98-1-0158 to RHW from the Office of Naval Research. We also thank the State of Florida for support of JJW, GAV, GJK, FMK, KAF, and RHW.

References

Atlas, E.L., Gordon, L.I., Hager, S.W., Park, P.K., 1971. A practical manual for use of the Technicon AutoAnalyzer in seawater nutrient analysis (revised). Department of Oceanography, Oregon State University, Corvallis, OR, pp. 1–49.

Baden, D.G., Mende, T.J., 1978. Glucose transport and metabolism in *Gymnodinium breve*. Phytochemistry 17, 1553–1558.

Blumberg, A.F., Mellor, G.L., 1987. A description of a three-dimensional coastal ocean circulation model. In: Heaps, N. (Ed.), Three Dimensional Coastal Ocean Models. AGU, Washington, DC, pp. 208–233.

Cannon, J.A., 1990. Development and dispersal of red tides in the Port River, south Australia. In: Graneli, E., Sundtrom, B., Edler, L., Anderson, D.M. (Eds.), Toxic Marine Phytoplankton. Elsevier, New York, NY, pp. 110–116.

Cervetto, G., Pagano, M., Gaudy, R., 1995. Feeding behavior and migrations in a natural population of the copepod *Acartia tonsa*. Hydrobiologia 300/301, 237–248.

Chew, F., 1956. A tentative method for the prediction of the Florida red tide outbreaks. Bulletin of Marine Science in the Gulf and the Caribbean 6 (4), 292–304.

Dagg, M.J., 1995. Ingestion of phytoplankton by the micro- and mesozooplankton communities in a productive subtropical estuary. Journal of Plankton Research 17 (4), 845–857.

Durbin, A.G., Durbin, E.G., Wlodarczyk, E., 1990. Diel feeding behavior in the marine copepod *Acartia tonsa* in relation to food availability. Marine Ecology Progress Series 68 (102), 23–45.

Easter, R.C., 1993. Two modified forms of Bott's positive-definite numerical advection scheme. Monthly Weather Review 121, 297–304.

Eppley, R.W., 1972. Temperature and phytoplankton growth in the sea. Fishery Bulletin 70, 1063–1085.

Fraga, S., Reguera, B., Bravo, I., 1990. *Gymnodinium catenatum* bloom formation in the Spanish rias. In: Graneli, E., Sundtrom, B., Edler, L., Anderson, D.M. (Eds.), Toxic Marine Phytoplankton. Elsevier, New York, NY, pp. 149–154.

Franks, P.J.S., 1992. Sink or swim: accumulation of biomass at fronts. Marine Ecology Progress Series 82, 1–12.

Fulton III, R.S., 1984. Distribution and community structure of estuarine copepods. Estuaries 7 (1), 38–50.

Gordon, L.I., Jennings, J.C., Ross, A.A., Krest, J.M., 1994. A suggested protocol for continuous flow automated analyses of seawater nutrients (phosphate, nitrate, nitrite, and silicic acid) in the WOCE Hydrographic Program and the Joint Global Ocean Fluxes Study. WOCE Operations Manual, WHP. Off. Rep. WHPO 91-1, WOCE Rep. 68/91. US World Ocean Circulation Experiment Office, College Station, TX, 120pp.

He, R., Weisberg, R.H., 2002. West Florida shelf circulation and temperature budget for the 1999 spring transition. Continental Shelf Research 22 (5), 719–748.

He, R., Weisberg, R.H., 2003. West Florida shelf circulation and temperature budget for the 1998 fall transition. Continental Shelf Research 23, 777–800.

Heil, C.A., 1986. Vertical migration of *Ptychodiscus brevis* (Davis) Steidinger. M.S. Thesis, University of South Florida, St. Petersburg, FL, p. 118.

Heil, C.A., Vargo, G.A., Spence, D.N., Neely, M.B., Merkt, R., Lester, K.M., Walsh, J.J., 2002. Nutrient stoichiometry of a *Gymnodinium breve* bloom: what limits blooms in oligotrophic environments? In: Proceedings of the IX International Symposium on Harmful Algal Blooms, Hobart, Australia, pp. 165–168.

Jeong, H.J., 1994. Predation effects of the calanoid copepod *Acartia tonsa* on a population of the heterotrophic dinoflagellate *Protoperidinium* cf. *divergens* in the presence of co-occurring red-tide dinoflagellate prey. Marine Ecology Progress Series 111, 87–97.

Kirk, J.T.O., 1994. Light and photosynthesis in aquatic ecosystems. Cambridge University Press, Cambridge, UK, p. 509.

Lenes, J.M., Darrow, B.P., Cattrall, C., Heil, C.A., Vargo, G.A., Callahan, M., Byrne, R.H., Prospero, J.M., Bates, D.E., Fanning, K.A., Walsh, J.J., 2001. Iron fertilization and the *Trichodesmium* response on the west Florida shelf. Limnology and Oceanography 46 (6), 1261–1277.

Lester, K.M., 2005. Zooplankton of the west Florida shelf: relationships with *Karenia brevis* blooms. Ph.D. Dissertation, University of South Florida, St. Petersburg, p. 216.

Li, Z., Weisberg, R.H., 1999a. West Florida continental shelf response to upwelling-favorable wind forcing: dynamics. Journal of Geophysical Research C. Oceans 104 (C10), 23427–23442.

Li, Z., Weisberg, R.H., 1999b. West Florida shelf response to upwelling-favorable wind forcing: kinematics. Journal of Geophysical Research C. Oceans 104 (C6), 13507–13527.

Lincoln, J.A., Turner, J.T., Bates, S.S., Leger, C., Gauthier, D.A., 2001. Feeding, egg production, and egg hatching success of the copepods *Acartia tonsa* and *Temora longicornis* on diets of the toxic diatom Pseudo-nitzschia multiseries and the non-toxic diatom Pseudo-nitzschia pungens. Hydrobiologia 453/454, 107–120.

Margalef, R., Estrada, M., Blasco, D., 1979. Functional morphology of organisms involved in redtides, as adapted to decaying turbulence. In: Taylor, D.L., Seliger, H.H. (Eds.), Toxic Dinoflagellate Blooms. Elsevier, New York, NY, pp. 89–94.

Mellor, G.L., Yamada, T., 1982. Development of a turbulence closure model for geophysical fluid problems. Reviews of Geophysics 20, 851–875.

Orlanski, I., 1976. A simple boundary condition for unbounded hyperbolic flows. Journal of Computational Physics 21, 251–269.

Pagou, K., Ignatiades, L., 1990. The peridoicity of *Gymnodinium breve* (Davis) in Saronicos Gulf, Aegean Sea. In: Graneli, E., Sundtrom, B., Edler, L., Anderson, D.M. (Eds.), Toxic Marine Phytoplankton. Elsevier, New York, NY, pp. 206–208.

Penta, B., 2000. Phytoplankton competition in the WFS: a simulation analysis with "red tide" implications. Ph.D. Dissertation, University of South Florida, St. Petersburg, FL, p. 259.

Pierce, R.H., Henry, M.S., Proffitt, L.S., Hasbrouck, P.A., 1990. Red tide toxin (brevitoxin) enrichment in marine aerosol. In: Graneli, E., Sundtrom, B., Edler, L., Anderson, D.M. (Eds.), Toxic Marine Phytoplankton. Elsevier, New York, NY, pp. 397–402.

Roach, P.J., 1976. Computational Fluid Dynamics. Hermosa Publications, Albuquerque, NM.

Rounsefell, G.A., Dragovich, A., 1966. Correlation between oceanographic factors and abundance of the Florida red tide (*Gymnodinium breve* Davis) during 1954–1961. Bulletin of Marine Science 16, 404–422.

Sakamoto, Y., Lockey, R.F., Krzanowski, J.J., 1987. Shellfish and fish poisoning related to toxic dinoflagellates. Southern Medical Journal 80, 866–870.

Satsmadjis, J., Friligos, N., 1983. Red tide in Greek waters. Vie et Melieu 33 (2), 111–117.

Shanley, E., 1985. Photoadaptation in the red tide dinoflagellate *Ptychodiscus brevis*. M.S. Thesis, University of South Florida, St. Petersburg, FL, p. 122.

Shanley, E., Vargo, G.A., 1993. Cellular composition, growth, photosynthesis, and respiration rates of *Gymnodinium breve* under varying light levels. In: Smayda, T.J., Shimizu, Y. (Eds.), Toxic Phytoplankton Blooms in the Sea. Elsevier, Amsterdam, pp. 831–836.

Shimizu, Y., Chou, H., Bando, H., 1986. Structure of Brevitoxin A (GB-1 Toxin), the most potent toxin in the Florida red tide organism *Gymnodinium breve* (*Ptychodiscus brevis*). Journal of the American Chemical Society 108, 514–515.

Shimizu, Y., Watanabe, N., Wrensford, G., 1995. Biosynthesis of brevitoxins and heterotrophic metabolism in *Gymnodinium breve*. In: Lassus, P., Arzul, G., Erard, E., Gentien, P., Marcaillou, C. (Eds.), Harmful Marine Algal Blooms. Lavoisier Intercept Ltd., Paris, pp. 351–357.

Simon, J.L., Dauer, D.M., 1972. A quantitative evaluation of red tide induced mass mortalities of benthic invertebrates in Tampa Bay, Florida. Environmental Letters 3, 229–234.

Smagorinsky, J., 1963. General circulation experiments with primitive equations. I: the basic experiment. Monthly Weather Review 91, 99–164.

Steele, J.H., 1962. Environmental control of photosynthesis in the sea. Limnology and Oceanography 7, 137–150.

Steidinger, K.A., 1973. Phytoplankton ecology: a conceptual view based on eastern Gulf of Mexico research. CRC Critical Review of Microbiology 3, 49–67.

Steidinger, K.A., 1975. Implications of dinoflagellate life cycles on initiation of *Gymnodinium breve* red tides. Environmental Letters 9, 129–139.

Steidinger, K.A., 1983. A re-evaluation of toxic dinoflagellate biology and ecology. Progress in Phycology Research 2, 147–188.

Steidinger, K.A., Haddad, K.D., 1981. Biologic and hydrographic aspects of red tides. Bioscience 31 (11), 814–819.

Steidinger, K.A., Ingle, R.M., 1972. Observations on the 1972 summer red tide in Tampa Bay, Florida. Environmental Letters 3, 271–278.

Stickney, R.R., Knowles, S.C., 1975. Summer zooplankton distribution in a Georgia estuary. Marine Biology 33, 147–154.

Taft, W.H., Martin, D.F., 1986. The potential for managing a Florida red tide. Journal of Environmental Science and Health A 21 (2), 107–127.

Tester, P.A., Steidinger, K.A., 1997. *Gymnodinium breve* red tide blooms: initiation, transport, and consequences of surface circulation. Limnology and Oceanography 42 (5), 1039–1051.

Turner, J.T., Tester, P.A., 1989a. Zooplankton feeding ecology: nonselective grazing by the copepods *Acartia tonsa* Dana, *Centropages velificatus* De Oliveira, and *Eucalanus pileatus* Giesbrecht in the plume of the Mississippi River. Journal of Experimental Marine Biology and Ecology 126, 21–43.

Turner, J.T., Tester, P.A., 1989b. Zooplankton feeding ecology: copepod grazing during an expatriate red tide. Coastal and Estuarine Studies 35, 359–374.

Turner, J.T., Tester, P.A., Hansen, P.J., 1998. Interactions between toxic marine phytoplankton and metazoan and protistan grazers. In: Anderson, D.M., Cembella, A.D., Hallegraeff, G.M. (Eds.), Physiological Ecology of Harmful Algal Blooms. Springer, Berlin.

Walsh, J.J., Penta, B., Dieterle, D.A., Bissett, P., 2001. Predictive ecological modeling of harmful algal blooms. Human and Ecological Risk Assessment 7 (5), 1369–1383.

Walsh, J.J., Haddad, K.D., Dieterle, D.A., Weisberg, R.H., Li, Z., Yang, H., Muller-Karger, F.E., Heil, C.A., Bissett, P.,

2002. A numercial analysis of landfall of the 1979 red tide of *Karenia brevis* along the west coast of Florida. Continental Shelf Research 22 (1), 15–38.

Walsh, J.J., Weisberg, R.H., Dieterle, D.A., He, R., Darrow, B.P., Jolliff, J.K., Lester, K.M., Vargo, G.A., Kirkpatrick, G.J., Fanning, K.A., Sutton, T.T., Jochens, A.E., Biggs, D.C., Nababan, B., Hu, C., Muller-Karger, F.E., 2003. Phytoplankton response to intrusions of slope water on the west Florida shelf: models and observations. Journal of Geophysical Research 108 (C6), 1–23.

Walsh, J.J., Jolliff, J.K., Darrow, B.P., Lenes, J.M., Milroy, S.P., Remsen, A., Dieterle, D.A., Carder, K.L., Chen, F.R., Vargo, G.A., Weisberg, R.H., Fanning, K.A., Muller-Karger, F.E., Shin, E., Steidinger, K.A., Heil, C.A., Tomas, C.R., Prospero, J.S., Lee, T.N., Kirkpatrick, G.J., Whitledge, T.E., Stockwell, D.A., Villareal, T.A., Jochens, A.E., Bontempi, P.S., 2006. Red tides in the Gulf of Mexico: where, when, and why. Journal of Geophysical Research C. Oceans 111 (C11) [np].

Weisberg, R.H., Black, B.D., Li, Z., 2000. An upwelling case study of Florida's west coast. Journal of Geophysical Research 105 (C5), 11459–11469.

Wilson, W.B., 1967. The suitability of seawater for the survival and growth of *Gymnodinium breve* Davis and some effects of phosphorus and nitrogen on its growth. Florida State University Professional Papers Series, Florida Board of Conservation, Tallahassee, FL, pp. 1–42.

Wright, S.W., Jeffrey, S.W., Mantoura, R.F.C., Llewellyn, C.A., Bjornland, T., Repeta, D., Welschmeyer, N., 1991. Improved HPLC method for the analysis of chlorophylls and carotenoids from marine phytoplankton. Marine Ecology Progress Series 77, 183–196.

Wyatt, T., 1990. Do algal blooms play homeostatic roles? In: Graneli, E., Sundtrom, B., Edler, L., Anderson, D.M. (Eds.), Toxic Marine Phytoplankton. Elsevier, New York, NY, pp. 249–252.

Yang, H., Weisberg, R.H., 1999. Response of the west Florida shelf circulation to climatological wind stress forcing. Journal of Geophysical Research 104 (C3), 5301–5320.